

My, how you've grown: a practical guide to modeling size transitions for Integral Projection Model (IPM) applications

Tom E.X. Miller^{*a} and Stephen P. Ellner^b

^aDepartment of BioSciences, Rice University, Houston, TX

^bDepartment of Ecology and Evolutionary Biology, Cornell University,
Ithaca, New York

Running header: Better growth modeling for IPMs

*Corresponding author. Department of BioSciences, Rice University, Houston, TX 77005-1827. Email:
tom.miller@rice.edu Phone: 713-348-4218

¹ **Abstract**

- ² 1. Integral Projection Models (IPMs) are widely used for studying the dynamics of
³ continuously size-structure populations. IPMs require a growth sub-model that
⁴ describes the probability of future size conditional on current size. Over the past
⁵ two decades, most IPM studies have assumed that this probability is normally-
⁶ distributed, despite repeated calls for non-Gaussian approaches that accommodate
⁷ skewness and kurtosis known to occur in size transition data.
- ⁸ 2. We provide a general workflow for modeling size transitions that accommodates
⁹ non-Gaussian growth patterns while retaining the desirable features (ecologically
¹⁰ important covariates and random effects) that Gaussian approaches typically pro-
¹¹ vide. Our approach emphasizes visual diagnostics of residuals from pilot Gaussian
¹² models and quantile-based metrics of skewness and kurtosis that vet the fit of the
¹³ Gaussian distribution and guide the selection of an alternative, if necessary. We
¹⁴ illustrate our methods by reanalyzing size transition data from our published IPM
¹⁵ studies, targeting a diversity of demographic quantities including population growth
¹⁶ rate, invasion wave velocity, and evolutionarily stable life history strategies.
- ¹⁷ 3. Across one coral and three plant case studies, skewness and excess kurtosis were
¹⁸ common features of size transition data and non-Gaussian growth models consis-
¹⁹ tently generated simulated data that were more consistent with the real data than
²⁰ pilot Gaussian models. However, in these case studies, the effects of “improved”
²¹ growth modeling on IPM results were generally modest, and differed in direction or
²² magnitude between different outputs from the same model.
- ²³ 4. Using tools that were not available when IPMs were first developed, it is now possi-
²⁴ ble to fit non-Gaussian models to size transition data without sacrificing ecological
²⁵ complexity; our worked examples demonstrate how, including open-access data and
²⁶ computing scripts. Doing so, as guided by careful interrogation of the data, will re-
²⁷ sult in a model that better represents the population for which it is intended.

²⁸ **Keywords**

29 Introduction

30 Structured demographic models – matrix and integral projection models (MPMs and
31 IPMs) – are powerful tools for data-driven modeling of population dynamics and via-
32 bility that are widely used in basic and applied settings. In contrast to MPMs for pop-
33 ulations with discrete structure (life stage, age class, etc.), IPMs (Easterling et al., 2000)
34 readily accommodate populations structured by continuous state variables, most com-
35 monly size. A related innovation of the IPM framework is its emphasis on regression-
36 based modeling for parameter estimation, which often carries important advantages for
37 making the most of hard-won data (Ellner et al., 2022).

38 A standard workflow allows ecologists to assemble an IPM from data using famili-
39 iar statistical tools to describe growth, survival, reproduction, and other demographic
40 transitions as functions of size (Coulson, 2012; Ellner et al., 2016). The relative ease of
41 the regression-based approach, accommodating multiple covariates (e.g., environmental
42 factors, experimental treatments) and complex variance structures (e.g., random effects,
43 correlated errors), has facilitated a growing body of IPM literature that examines how
44 biotic or abiotic factors affect population dynamics (e.g., Louthan et al., 2022; Ozgul
45 et al., 2010; Schultz et al., 2017) and explores the consequences of demographic hetero-
46 geneity associated with spatial, temporal, and individual variation (e.g., Compagnoni
47 et al., 2016; Crone, 2016; Plard et al., 2018). The vital rate regressions (or “sub-models”)
48 are the bridge between the individual-level data and the population-level model and its
49 predictions; it is important to get them right.

50 Compared to other vital rates, growth is special. The regression sub-models for
51 survival and reproduction only need to provide a single mean value as functions of
52 size (we use “size” as the name for whatever continuous variable defines the population
53 structure, which could instead be immune competence, mother’s weight, etc.). But for
54 modeling growth, the full probability distribution of subsequent size, conditioned on
55 initial size, must be defined. This distribution defines the growth ‘kernel’ $G(z', z)$ that
56 gives the probability density of any future size z' at time $t + 1$ conditional on current size
57 z at time t . Whenever survival and reproduction are size-dependent, the entire distribu-
58 tion of size transitions can strongly influence IPM predictions because this distribution
59 governs how frequently size changes are much greater or much lower than average.

60 The original template for modeling size transitions in IPMs was provided by East-
61 erling et al. 2000. They first tried simple linear regression, assuming normally dis-
62 tributed size changes with constant variance. Because the residuals from this regression
63 exhibited non-constant variance, they used a two-step approach that estimated the size-

64 dependence in the residual variance (better options soon became available, such as the
65 `lme` function in R). However, even after accounting for non-constant variance, growth
66 data may still deviate from the assumption that size transitions are normally distributed.
67 Size transitions are often skewed such that large decreases are more common than large
68 increases (Peterson et al., 2019; Salguero-Gómez and Casper, 2010), or vice versa (Stub-
69 berud et al., 2019). Size transitions may also exhibit excess kurtosis ('fat tails'), where
70 extreme growth or shrinkage is more common than predicted by the tails of the normal
71 distribution (Hérault et al., 2011).

72 The observation that the normal distribution may poorly describe size transitions
73 in real organisms has been made before, and several studies have emphasized that al-
74 ternative distributions should be explored (Easterling et al., 2000; Peterson et al., 2019;
75 Rees et al., 2014; Williams et al., 2012). Nonetheless, default use of Gaussian growth
76 distributions (often with non-constant variance) remains the standard practice. The gen-
77 eral state-of-the-art in the literature appears to remain where it was 20 or so years ago,
78 using the default model without pausing to examine critically whether or not it actually
79 provides a good description of the data. We are guilty of this, ourselves.

80 The persistence of Gaussian growth modeling is understandable. There is a long
81 tradition of statistical modeling built on the assumption of normally distributed resid-
82 uals with constant variance. Popular packages such as `lme4` (Bates et al., 2007), `mgcv`
83 (Wood, 2017), and `MCMCglmm` (Hadfield et al., 2010) make it easy to fit growth models
84 with potentially complex fixed- and random-effect structures, but the possible distribu-
85 tions of continuous responses are limited, and default to Gaussian. Abandoning these
86 convenient tools for the sake of more flexible growth modeling means, it may seem,
87 sacrificing the flexibility to rigorously model diverse and potentially complex sources of
88 variation in growth, some of which may be the motivation driving the study in the first
89 place.

90 The question we address here is: how can ecologists escape the apparent trade-off
91 between realistically capturing the variance, skew, and kurtosis of size transition data
92 on the one hand, and flexibly including the multiple covariates and random effects that
93 often have substantial impacts on demographic rates? In this article, we offer an answer.

94 Our goal here is to present and illustrate a general and practical "recipe" that moves
95 growth modeling past the standards set over 20 years ago, using software tools available
96 now.¹ Like any recipe, users may need to make substitutions or add ingredients to
97 suit their situation. Our approach emphasizes graphical diagnostics for developing and

¹Our statements about what is available now are based on what tools reliably deliver in our experience, not on what they promise.

98 evaluating growth models, rather than a process centered on statistical model selection.
99 Through a set of empirical case studies we demonstrate how a simple workflow, using
100 tools that were nonexistent or not readily available when IPMs first came into use, makes
101 it straightforward and relatively easy to identify when the default model is a poor fit to
102 the data, and to then choose and fit a substantially better growth model that is no harder
103 to use in practice. We illustrate our approach by revisiting published IPM analyses that
104 assumed Gaussian growth, including our own previous work. In each case, the Gaussian
105 assumption does not stand up to close scrutiny. We illustrate how we could have done
106 better, and the consequences of “doing better” for our ecological inferences. All of our
107 analyses may be reproduced from code and data that are publicly available (see Data
108 accessibility statement).

109 A workflow for growth modeling

110 The modeling workflow that we suggest runs as follows (Fig. 1):

- 111 1. *Fit a “pilot” model or models assuming a Gaussian distribution, but allowing for non-*
112 *constant variance.*

113 This step is familiar to most IPM users, as it is the start and end of the traditional
114 workflow. A well-fitted Gaussian model accurately describes the mean and variance
115 of future size conditional on current size and possibly on other measured covari-
116 ates or random effects. This step may include model selection to identify which
117 treatment effects or environmental drivers affect the mean and/or variance of future
118 size. Non-constant variance is often fitted in a two-stage process, first fitting mean
119 growth assuming constant variance, then doing a regression relating the squared
120 residuals to initial size or the fitted mean of subsequent size. Fitting mean and
121 variance simultaneously, as can be done with R packages **mrgcv** and **nmle**, is ad-
122 vantageous when possible because incorrectly assuming constant variance can affect
123 model selection for the mean. But two-step fitting may be convenient when there
124 are multiple fixed and random effects that can affect growth variance, because the
125 fitted mean value implicitly accounts for all of them. We illustrate both one-step and
126 two-step approaches in the case studies below.

127 Allowing non-constant variance removes the need for transforming the data to
128 stabilize the growth variance. Transformation remains an option when it does not
129 create new problems (see Discussion), and it may have advantages besides variance

130 stabilization. In particular log-transformation is often appropriate for size data (Ell-
131 ner et al., 2016), and it helps to avoid eviction at small sizes.

- 132 2. *Use statistical and graphical diagnostics to identify if and how the standardized residuals*
133 *deviate from Gaussian, and to identify a more appropriate distribution.*

134 If the Gaussian pilot model is valid, the set of standardized residuals (standardized
135 by the standard deviation) should be Gaussian with mean zero and unit variance,
136 with no skew or excess kurtosis. This criterion provides a straightforward test for
137 whether to accept a Gaussian growth model or explore alternatives. If the standard-
138 ized residuals are satisfactorily Gaussian, skip to the final step of the workflow.

139 There are many ways that growth data may deviate from Gaussian, and the na-
140 ture of those deviations can guide the search for a better distribution. Frequentist
141 tests such as the D'Agostino test of skewness (D'Agostino, 1970) and the Anscombe-
142 Glynn test of kurtosis (Anscombe and Glynn, 1983) could be used to diagnose
143 whether the aggregate distribution of standardized residuals deviates from normal-
144 ility (R package **moments** (Komsta and Novomestky, 2015)). However, the aggregate
145 distribution of standardized residuals may be misleading if properties such as skew
146 and kurtosis vary with size or other covariates. For example, a change in the di-
147 rection of skewness from small to large sizes might produce zero overall skewness,
148 but really requires a distribution flexible enough to accommodate both positive and
149 negative skew, such as the skewed normal or Johnson S_U distributions. Alterna-
150 tively, growth data may lack skew but may exhibit leptokurtosis (in which case the t
151 distribution may be a good choice) or may shift from platykurtosis to leptokurtosis
152 depending on initial size (in which case the power exponential distribution may be
153 a good choice). It is therefore essential to visualize trends in distribution properties
154 with respect to size, either initial size (for simple models with only size-dependence)
155 or expected future size (for models with multiple fixed effects). In the case studies
156 below, we rely on quantile regression of the standardized residuals to visualize skew
157 and kurtosis as continuous functions of initial size or expected future size. Fig. 1
158 includes guidance on how the skew and kurtosis properties of the standardized
159 residuals suggest options for an appropriate growth distribution. In our case stud-
160 ies we take advantage of the many distributions provided in the **gamlss** R package
161 (Stasinopoulos et al., 2007), but any other distributions with the necessary properties
162 can be used.

- 163 3. *Refit the growth model using the chosen distribution.*

164 In models with multiple covariates and/or random effects, each potentially affecting

several distribution parameters (location, scale, skew, kurtosis) in different ways, “refit the model” could entail a massive model selection process to identify the “right” or “best” non-Gaussian model. And with so many options, model uncertainty may be overwhelming and over-fitting becomes a significant risk even if precautions against it are taken. We therefore argue for adopting the more modest goal of remedying any evident defects in the Gaussian model. As we demonstrate below, the functional forms for the mean and standard deviation (or location and scale parameters) can often be carried over from the pilot Gaussian model into a non-Gaussian distribution, leaving skew and kurtosis as the targets for improvement.

Our recommendation for this step is based on the fact that parameter estimation using Gaussian regression models is generally robust to deviations from normality (Schielzeth et al., 2020), meaning that the mean of the Gaussian model is probably a good proxy for the mean of the non-Gaussian model (and if it is not, the next step in the workflow would catch that). The functional forms for skew and kurtosis of the non-Gaussian model can be guided by the qualitative features of the graphical diagnostics (e.g., skewness switches from positive to negative with size).

4. *Test the final model through graphical diagnostics comparing simulated and real growth data.* A good model will generate simulated data that look like the real data. Again, it is important to inspect the properties of simulated data conditional on initial size or expected future size, rather than examining the aggregate distribution. We provide examples below of informative comparisons between simulated and real data, based mainly on quantiles. If the simulated data do not correspond well with real data, alternative (possibly more flexible) growth distributions should be explored, or more complex functions relating distribution parameters to current size and other covariates. However, we again caution against a full-blown model selection exercise. Instead, alternative models should be chosen to remedy observable discrepancies between real and simulated size transition data, and at most slightly modified based on final diagnostics and statistical tests.

How should skewness and kurtosis be measured?

Improvement of a Gaussian model will involve scrutiny of skewness and kurtosis, so measurement of these properties warrants some attention. The standard measures of skewness and kurtosis (tail thickness) are based on the third and fourth central moments,



Figure 1: General workflow of recommendations for IPM growth modeling (left) and guide to common non-Gaussian distributions of size x for $x \in \mathbb{R}$ that can accommodate different combinations of skewness and kurtosis (right). All of these distributions (often including multiple versions or parameterizations of each) are available in the package `gamlss.dist`, except for the skewed generalized t , which is available in the package `sgt` (Davis, 2015).

197 respectively, of the distribution:

$$198 \quad \text{Skewness} = \frac{m_3}{\sigma^3}, \quad \text{Excess kurtosis} = \frac{m_4}{\sigma^4} - 3 \quad (1)$$

199 where $m_k = \mathbb{E}(X - \bar{X})^k$ is the k^{th} central moment of a random quantity X and σ^2 is the
200 variance (second central moment). A Gaussian distribution has zero skewness and zero
201 excess kurtosis.

202 The standard measures are easy to calculate but their use for choosing and eval-
203 uating growth models is hindered by their poor sampling properties. Because empirical
204 estimates involve high powers of data values, a few outliers can produce very inaccurate
205 estimates. Figure 2 shows a simulated example, where the underlying “data” are a sam-

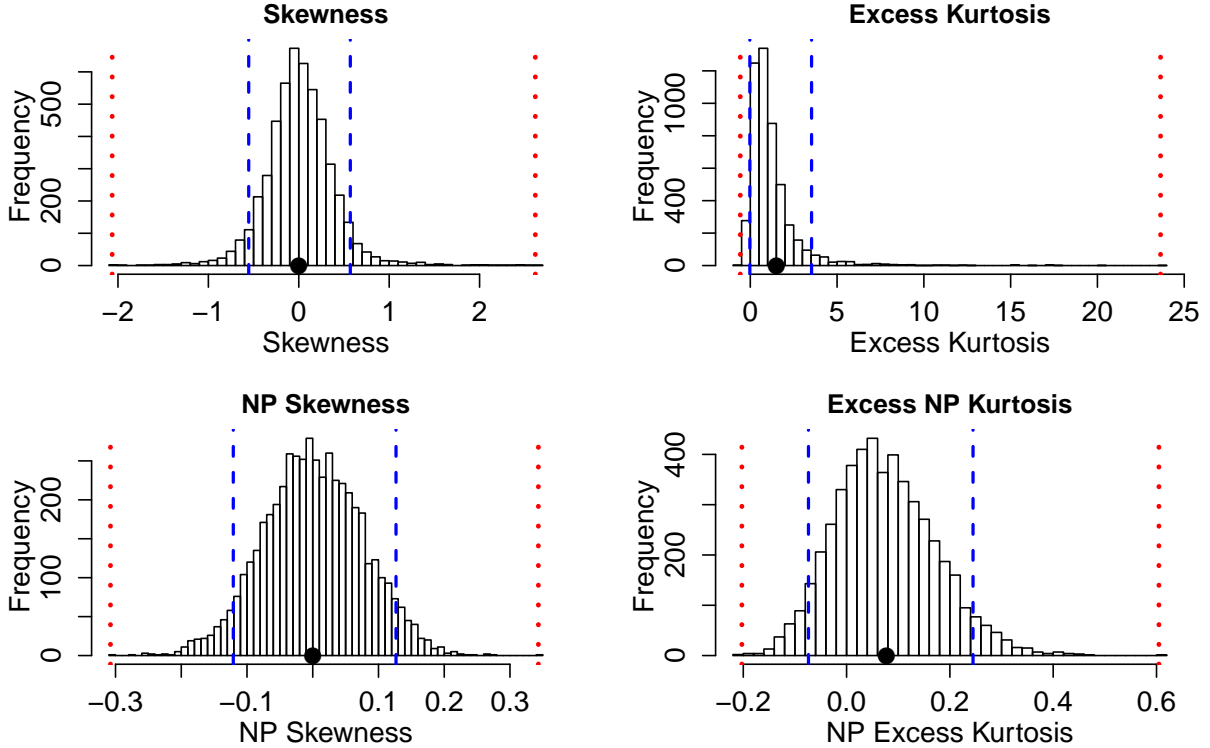


Figure 2: Histograms of skewness and kurtosis estimates using moment-based definitions (top two panels), compared with the nonparametric measures based on quantiles (bottom two panels). Note the very large differences in scale. Histograms are based on 5000 replicate draws of a sample of 200 independent values, from a t distribution with 8 degrees of freedom. Dotted red vertical lines mark the minimum and maximum of sample estimates, and dashed blue lines show the 5th and 95th percentiles. The true value is indicated by a black dot on the x -axis. Figure drawn by script `NPmoments.R`

ple of size 200 from a t distribution with 8 degrees of freedom; the true skew is 0, and the true excess kurtosis is 1.5. The distance between the largest and smallest estimates (indicated by the dotted red vertical lines), relative to the distance between the 5th and 95th percentiles, shows the broad extent of extreme values that can occur even with a large sample, especially for kurtosis.

We therefore use nonparametric (NP) measures of skew and kurtosis that are based on quantiles and thus are less sensitive to a few extreme values. Let q_α denote the α quantile of a distribution or sample (e.g., $q_{0.05}$ is the 5th percentile). For any $0 < \alpha < 0.5$, a quantile-based measure of skewness is given by (McGillivray, 1986)

$$\text{NP Skewness} = \frac{q_\alpha + q_{1-\alpha} - 2q_{0.5}}{q_{1-\alpha} - q_\alpha}. \quad (2)$$

216 NP Skewness measures the asymmetry between the tails of the distribution above and
 217 below the median. The size of the upper tail can be measured (for any $0 < \alpha < 0.5$) by
 218 $\tau_U = q_{1-\alpha} - q_{0.5}$; for $\alpha = 0.05$ this is the difference between the 95th percentile and the
 219 median. The lower tail size is $\tau_L = q_{0.5} - q_\alpha$. The definition above is equivalent to

$$220 \quad \text{NP Skewness} = \frac{\tau_U - \tau_L}{(\tau_U + \tau_L)}. \quad (3)$$

221 An NP Skewness of ± 0.2 says that the difference in tail sizes is 20% of their total. The
 222 range of possible values is -1 to 1. Both $\alpha = 0.25$ (sometimes called “Kelly’s skewness”) and
 223 $\alpha = 0.1$ (“Bowley’s skewness”) are common choices. We used $\alpha = 0.1$, unless
 224 otherwise stated.

225 An analogous quantile-based measure of kurtosis (Jones et al., 2011) is

$$226 \quad \text{NP Kurtosis} = \frac{q_{1-\alpha} - q_\alpha}{q_{0.75} - q_{0.25}}. \quad (4)$$

227 For $\alpha = 0.05$, NP Kurtosis is the difference between the 95th and 5th percentiles, relative
 228 to the interquartile range. To facilitate interpretation, we scale NP Kurtosis relative to
 229 its value for Gaussian distribution, and subtract 1 so that the value for a Gaussian is
 230 zero. We call this “NP Excess Kurtosis”. The value for a Gaussian distribution is zero. A
 231 value of ± 0.2 means that the tails are on average 20% heavier (or lighter) than those of
 232 a Gaussian with the same interquartile range. We calculate NP Kurtosis using $\alpha = 0.05$
 233 unless otherwise stated, to focus on the tail edges, but again this is somewhat arbitrary.

234 Figure 2C,D illustrate how, applied to exactly the same simulated samples, the non-
 235 parametric measures produce a smaller fraction of highly inaccurate estimates caused
 236 by a few extreme values in the sample. But also note that, in contrast to the moment-
 237 based measures, numerically small values of the nonparametric measures (e.g., 0.1 or 0.2)
 238 should not be disregarded, because they are both scaled so that a value of 1 indicates
 239 extremely large departures from a Gaussian distribution.

240 Quantile-based estimation of skewness and kurtosis carries the added value that
 241 quantile regression methods may be used to derive these properties of size transitions
 242 as continuous functions of initial size or expected future size. In the examples below,
 243 we sometimes use the **qgam** package to fit smooth additive quantile regression models,
 244 which have the flexibility to accommodate nonlinear size-dependence in skewness and
 245 kurtosis. One risk of a gam-based approach is that fitted quantiles may be too “wiggly”
 246 without constraints on their complexity. In the examples below, we limit complexity by
 247 fitting splines with $k = 4$ or $k = 6$ basis functions. For the gam-averse, other quantile
 248 regression models may be equally suitable, and we illustrate those, too. For consistency

249 with nonparametric skewness and kurtosis, in comparisons of real and simulated data
 250 below, we use quantile-based measures of location and scale, and use quantile regression
 251 to visualize these as functions of size. Specifically, following Wan et al. (2014),

$$252 \quad \text{NP Mean} = \frac{q_{0.25} + q_{0.5} + q_{0.75}}{3} \quad (5)$$

253 and

$$254 \quad \text{NP SD} = \frac{q_{0.75} - q_{0.25}}{1.35}. \quad (6)$$

255 1 Case study: Sea fan corals, *Gorgonia ventalina*

256 We begin with a simple example where current size is the only predictor of future size.
 257 Bruno et al. (2011) developed an IPM to understand the rise and fall of a fungal pathogen
 258 *Aspergillus sydowii* in Caribbean sea fan corals *G. ventalina*. The model was based on re-
 259 peated observations of marked corals in permanent transects at several sites near Aku-
 260 mal, Mexico, recording disease status (infected/uninfected) and the area of uninfected
 261 tissue. The epidemic peak had passed and disease incidence was already low, so in-
 262 fected fans were relatively infrequent. We therefore limit the analysis here to uninfected
 263 individuals. Bruno et al. (2011) found statistically significant year and site effects, but
 264 as those explained a very small fraction of the variation in growth increments, they
 265 fitted a single growth model to data pooled across years and sites. We do the same
 266 here. The pooled data set consists of 358 observed size transitions. The data exhibited
 267 size-dependent variance in growth (change in area, cm^2). Bruno et al. (2011) chose to sta-
 268 bilize the variance by cube-root transforming size, and then fitting the standard model
 269 with Gaussian growth increments. Here we take a different approach, using natural log
 270 transformation of area and modeling size-dependent variance.

271 With initial size as the only predictor, a simple way to fit a Gaussian model with
 272 nonconstant variance is the `gam` function in `mgcv` library (Wood, 2017) using the `gaulss`
 273 family. The mean and standard deviation are both fitted as smoothing spline functions
 274 of initial size, and the `predict` function returns the fitted mean and also the inverse of
 275 the fitted standard deviations with which we can compute the scaled residuals:

```
276 # XH is a data frame holding the data
277 # logarea.t0, .t1 denote initial and final values of log-transformed area
278 fitGAU <- gam(list(logarea.t1~ s(logarea.t0), ~ s(logarea.t0)),
279                 data=XH, gamma=1.4, family=gaulss())
280 fitted_all = predict(fitGAU, type="response");
```

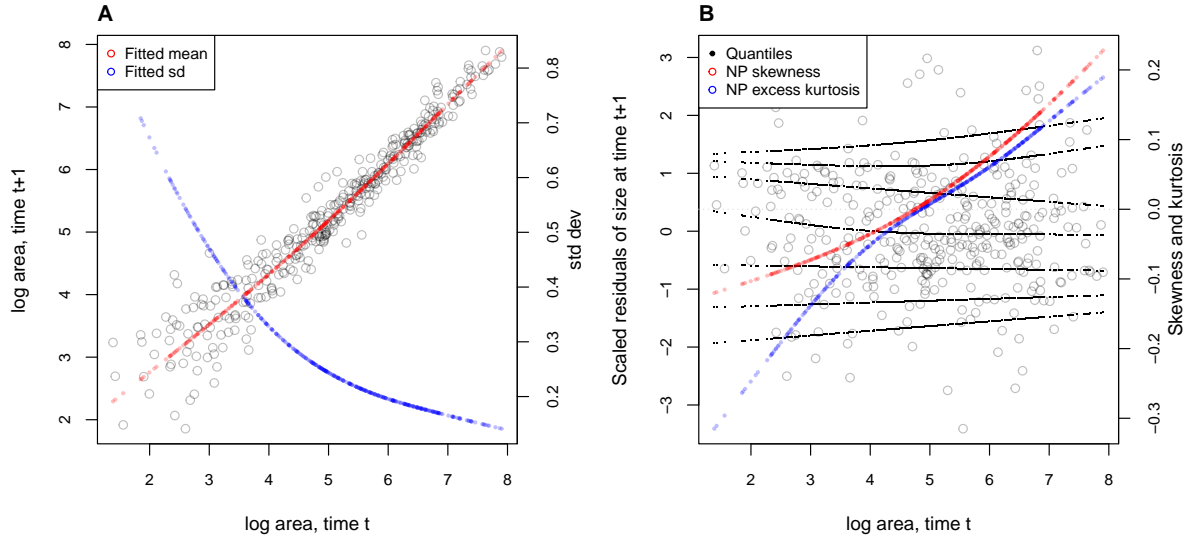


Figure 3: **A**, Size transition data for sea fan corals, *Gorgonia ventalina*, and fitted gam with mean (red) and standard deviation (blue) of future size conditional on current size. **B**, Quantile regressions of scaled residuals on size and nonparametric estimates of skewness (red) and excess kurtosis (blue) derived from them. Black lines in **B** show the 5th, 10th, 25th, 50th, 75th, 90th, and 95th quantiles. Figure made by script AkumalCorals_qgam.R.

```

281     fitted_sd = 1/fitted_all[,2];
282     scaledResids = residuals(fitGAU,type='response')/fitted_sd;

```

283 Fig. 3A shows the log-transformed data and Gaussian model. The mean function (solid
284 red curve) is visually nearly linear, but the fitted spline is strongly favored over a linear
285 model for the mean ($\Delta AIC \approx 9$). The spline for standard deviation σ versus initial size
286 reflects the evident greater variability in growth at smaller sizes.

287 There are no blatant signs of trouble in the pilot Gaussian model, but quantile re-
288 gressions on the scaled residuals, and the NP Skewness and Kurtosis metrics derived
289 from them (Eq. 3 and 4), suggest deviations from normality (Fig. 3B). Specifically, skew-
290 ness switches from negative to positive across the size range, with smaller corals more
291 prone to extreme shrinkage and larger corals more prone to extreme growth. Kurto-
292 sis also changes direction over the size distribution, with thinner tails than Gaussian at
293 small sizes and fatter tails at large sizes. The fitted nonparametric moments suggest that
294 the upper and lower tails of size transition probabilities may differ by up to 20%, and
295 the weight of the tails may be 20% greater or less than Gaussian, depending on initial
296 size – not overwhelming deficiencies, but not trivial either. Are these deviations from
297 normality severe enough to warrant a second, non-Gaussian iteration of growth mod-

eling? To answer that question, we simulated data from the fitted Gaussian model and examined whether key properties of the simulated data are consistent with those of the real data – this is the ultimate litmus test for a growth model’s adequacy and should be a standard element of IPM construction, in our opinion. If the simulated data are not consistent with the real data, it is time to choose a better distribution (Fig. 1). In this case, most of 100 Gaussian model simulations are out of line with the skew at smallest and largest sizes, and excess kurtosis observed at moderately large sizes (Fig. 4 CD). For at least some parts of the size distribution, a non-Gaussian model would better capture size transitions.

We sought a distribution that could accommodate the observed changes in the sign of skewness and excess kurtosis. We chose the sinh-arcsinh (SHASH) distribution, a four-parameter distribution that, conveniently, is included in **mgcv**’s **gam()** function. For consistency with the Gaussian for location and scale, specification of basis functions ($k = 4$) is limited to parameters for skewness and kurtosis:

```
312 fitSHASH <- gam(list(logarea.t1 ~ s(logarea.t0), # <- location  
313 ~ s(logarea.t0), # <- log-scale  
314 ~ s(logarea.t0,k=4), # <- skewness  
315 ~ s(logarea.t0,k=4)), # <- log-kurtosis  
316 data = XH, gamma = 1.4, family = shash, optimizer = "efs")
```

The fitted model’s mean and variance are nearly identical to the Gaussian (Fig. 4AB), and the fitted trends in skewness and kurtosis are much less “wiggly” than the estimate from the data (Fig. 4CD). Nonetheless, data simulated from the SHASH model are more consistent with the real data, with more SHASH data sets matching or exceeding the largest skewness and kurtosis values observed (Fig. 4CD). If one cares to quantify the difference between models, the SHASH model is clearly favored by AIC ($\Delta AIC = 5.45$) despite having twice as many parameters to fit.

What, then, have we gained by fitting a better growth model? Fig. 5A compares the predicted distributions of subsequent size in the fitted model and Gaussian pilot models, for the median size of a new recruit (leftmost pair of curves), the median initial size (central curves), and the 95th percentile of initial size in the data (rightmost curves). The differences are small, and most pronounced for the smallest size, where recruits are predicted to grow slightly larger under the SHASH model than the Gaussian model. The direction of this difference was surprising, because the SHASH has negative skew at small sizes in the data. However, the SHASH model also gives a better prediction of mean growth at small sizes than the Gaussian model. At intermediate sizes the

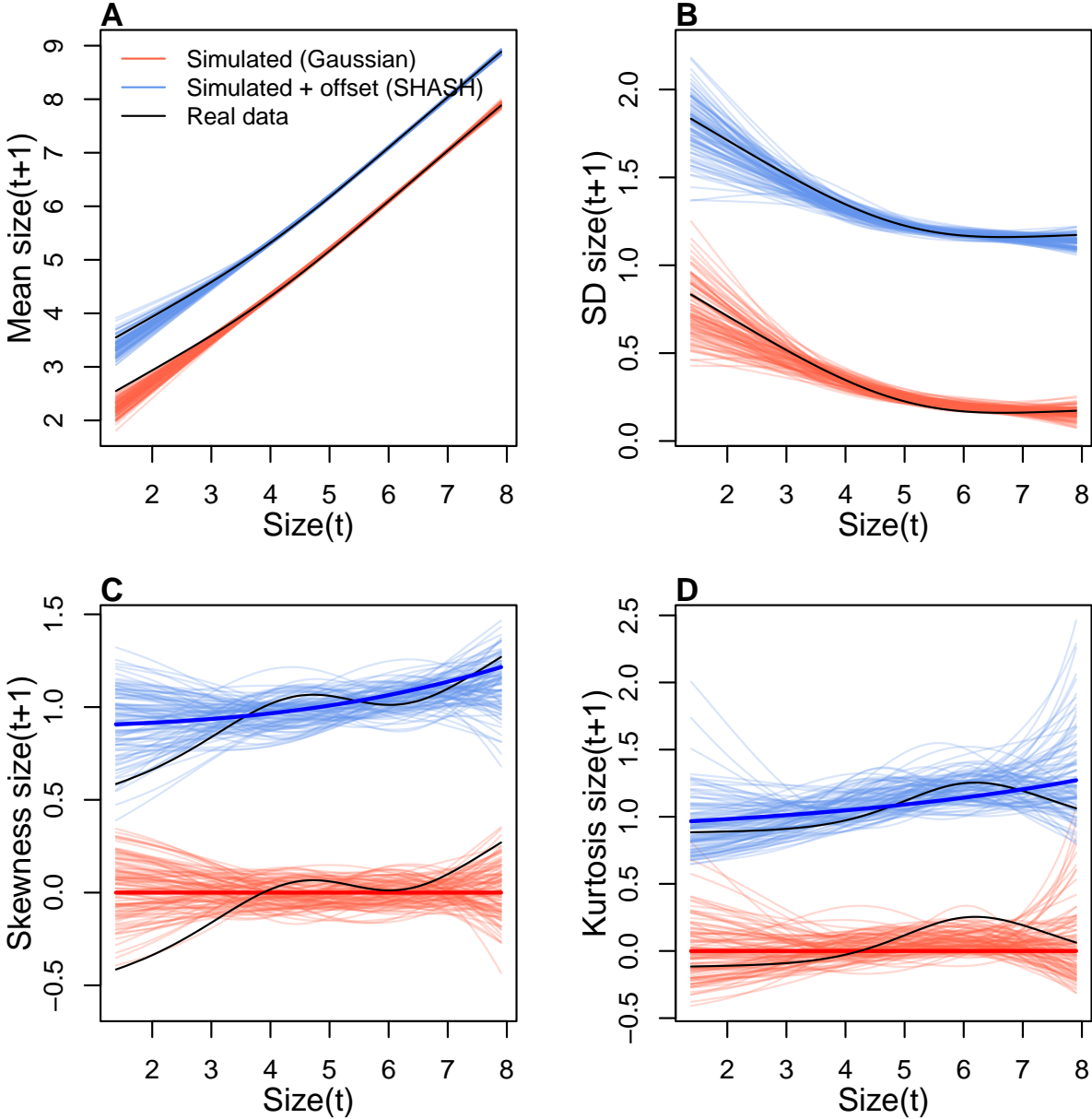


Figure 4: Comparisons among real coral data and data simulated from Gaussian and SHASH growth models for mean, standard deviation, NP skewness, and NP excess kurtosis of future size conditional on current size. Note that plotted values for the SHASH are offset by one unit to allow comparisons. In the skewness and kurtosis panels, the darker solid curves show the values for the fitted growth models. Figure made by script AkumalCorals_qgam.R.

³³³ predictions are nearly identical; at large sizes the SHASH has slightly lower standard deviation, but fatter tails (excess kurtosis). Fig. 5B shows the predicted steady-state size distributions resulting from a constant unit input of recruits. Again, the differences are

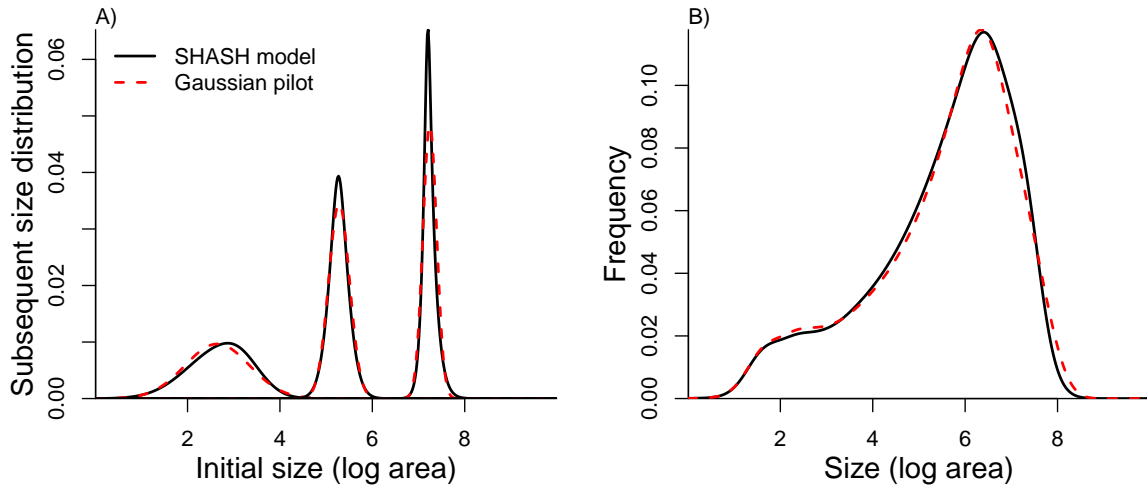


Figure 5: Comparisons between the fitted SHASH growth model (solid black curves) and the Gaussian pilot model (dashed red curves) for sea fans *G. ventalina*. A) Predicted frequency distributions of size in year $t + 1$ for three different values of size in year t . The leftmost pair of curves are for initial size equal to the median size of a new recruit (data from (Bruno et al., 2011)); central pair is for the median initial size of uninfected individuals; rightmost pair are for the 95th percentile initial size for uninfected individuals. B) Steady-state size distributions resulting from a constant unit input of new recruits. As in Bruno et al. (2011) we assume that larvae are very widely dispersed, so that the number of recruits arriving at any one location is independent of the local population abundance or structure. Size distribution of recruits was described by a kernel density estimate based on the measured sizes of known new recruits ($n = 9$). Figure made by script AkumalCoralsIPMs.R.

336 very subtle. Finally, the Gaussian and SHASH growth models predict very similar mean
 337 life span (17.7 and 17.9 years, respectively).

338 From these outputs, there is little evidence that improved modeling of coral growth
 339 meaningfully improved biological inferences from the IPM. One could argue that it was
 340 not worth the trouble, even though it was almost no trouble at all. But before fitting
 341 the SHASH model, we could not have known whether or not it would have made a
 342 difference.

343 In this case study we used `gam` to fit both the Gaussian and SHASH models because
 344 that obviated model selection on functions for mean, variance, and higher moments.
 345 However, `gam` should be used with caution. Nonparametric regression models notori-
 346 ously “wag their tails” because the ends of the fitted curve can be pulled close to the
 347 outermost data points. This is especially problematic for growth modeling, because data
 348 are typically sparse near the bounds of the size distribution. To minimize the risk of
 349 overfitting we specified the number of “knots” ($k=4$) and used `gamma=1.4` to overweight

350 model degrees of freedom as suggested by Gu (2013, sec. 3.2). But it is always impor-
351 tant to plot the fitted splines and make sure they do not wag unrealistically. If they do,
352 parametric regression may be a better choice.

353 2 Case study: lichen, *Vulpicida pinastri*

354 Growth data for the epiphytic lichen *Vulpicida pinastri* was first analyzed by Shriver
355 et al. 2012 and analyzed again by Peterson et al. 2019 in their study of negatively
356 skewed growth distributions. We therefore had an *a priori* expectation of deviation from
357 normality. The authors of the original study used a mixture distribution that separated
358 “normal growth or shrinkage” from “extreme shrinkage”. We aimed to fit a single,
359 flexible growth model that could realistically accommodate both types of size transition
360 without requiring *ad hoc* decisions about which observations were or were not “extreme”.
361 The data set includes 1,542 inter-annual transitions in thallus area (cm^2) observed from
362 2004 to 2009 in Kennicott Valley, AK.

363 For a pilot Gaussian model, following a bit of model selection, we again used the
364 `gaulss` family in `mgcv` to fit the mean and standard deviation of future size as second-
365 order polynomials of current size. As expected based on previous analyses, visual anal-
366 ysis of the standardized residuals indicated negative skew, especially at larger sizes, and
367 positive excess kurtosis (Fig. 6).

368 3 Case study: tree cholla cactus, *Cylindriopuntia imbricata*

369 The next case study, focusing on the tree cholla cactus *Cylindriopuntia imbricata* at the
370 Sevilleta Long-Term Ecological Research site in central New Mexico, adds a new feature
371 on top of the simple size-dependent regressions in the previous study: random effects
372 associated with temporal (year) and spatial (plot) environmental heterogeneity. This
373 long-term study of cactus demography was initiated in 2004 and different subsets of
374 the data have been analyzed in various IPM studies, all using Gaussian growth kernels
375 (Compagnoni et al., 2016; Czachura and Miller, 2020; Elderd and Miller, 2016; Miller
376 et al., 2009; Ohm and Miller, 2014). In fact, (Elderd and Miller, 2016) presented a Gaus-
377 sian growth model fit to the cactus data as an example of a well fit growth function,
378 based on a marginal distribution of residuals that appeared approximately Gaussian
379 and posterior predictive checks (PPCs) of a Bayesian model that suggested consistency

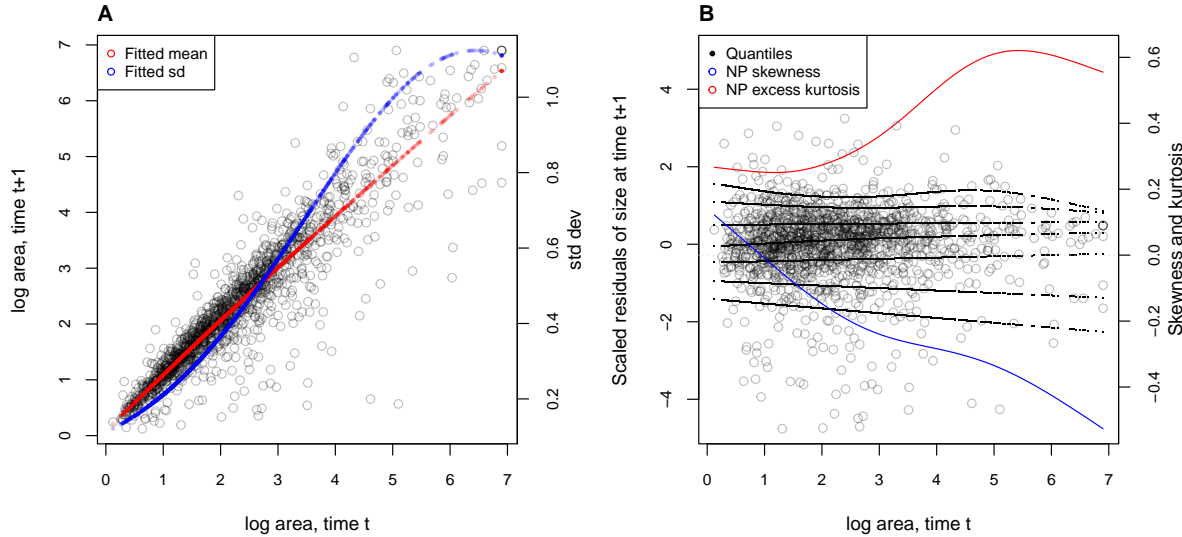


Figure 6: **A**, Size transition data for lichens, *Gorgonia ventalina*, and fitted gam with mean (red) and standard deviation (blue) of future size conditional on current size. **B**, Quantile regressions of scaled residuals on size and nonparametric estimates of skewness (red) and excess kurtosis (blue) derived from them. Black lines in **B** show the 5th, 10th, 25th, 50th, 75th, 90th, and 95th quantiles. Figure made by script `Vulpicida_IPMS.R`.

380 between the real data and data simulated from the fitted model (Fig. 4 in (Elderd and
381 Miller, 2016)).

382 While PPCs and the associated “Bayesian P-value” are popular diagnostic tools,
383 they are often considered to be too conservative (Conn et al., 2018; Zhang, 2014), failing
384 to reject marginally bad models even though they are very effective in rejecting models
385 that are terrible. The choice of discrepancy function (the statistic used to compare real
386 and simulated data) can also be limiting: in our previous work, we used a discrepancy
387 function focused on variance (the sum of the squared residuals), so we had a built-in
388 blind-spot for mismatches in higher moments. In the clarity of hindsight, the PPC gave
389 a false sense of security; the Gaussian was a poor choice all along.

390 The data for this new analysis include 4844 size transition observations from 929 in-
391 dividuals spanning 13 transition years (2004–2018) and 11 spatial replicates (three spatial
392 blocks in years 2004–2008 and eight 30m-by-30m plots in years 2009–2018). The data are
393 provided in Miller (2020). Following previous studies, we quantified size as the natural
394 logarithm of plant volume (cm^3), derived from height and width measurements.

395 We begin the growth modeling workflow, as above, with a generalized additive
396 model with the mean and standard deviation of size in year $t + 1$ modeled as function
397 of size in year t , with random intercepts for year and plot and assuming normally dis-

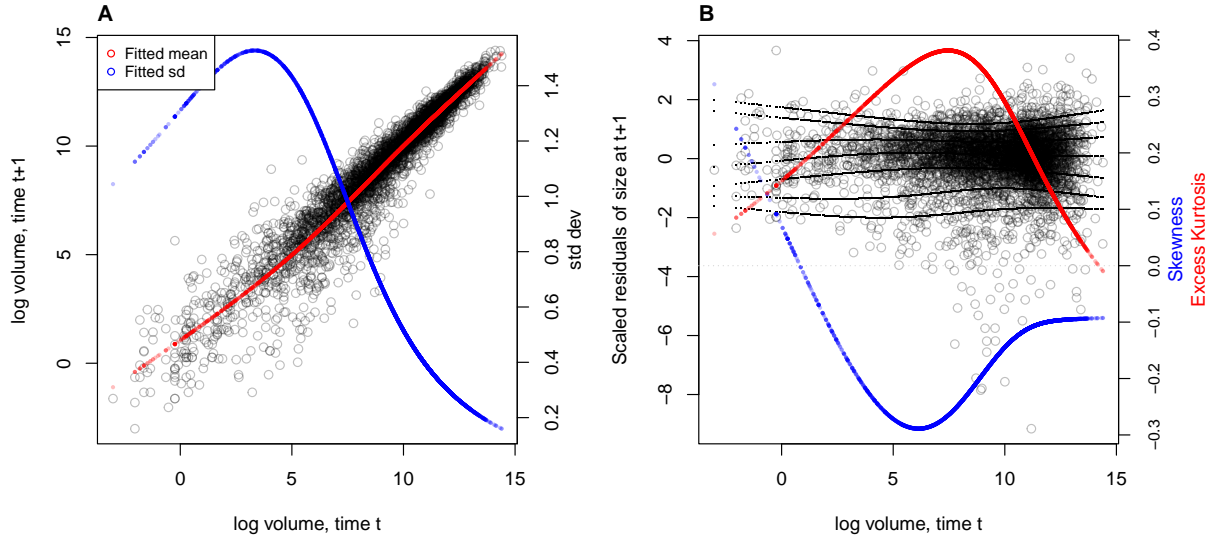


Figure 7: **A**, Size transition data for tree cholla cacti, *Cylindropuntia imbricata*, and fitted gam with mean (red) and standard deviation (blue) of future size conditional on current size. **B**, Quantile regressions of scaled residuals on size and nonparametric estimates of skewness (red) and excess kurtosis (blue) derived from them. Black lines in **B** show the 5th, 10th, 25th, 50th, 75th, 90th, and 95th quantiles. Figure made by script `cactus_growth_modeling_qgam.R`.

tributed residuals (`family=gaulss()`). The standardized residuals, accounting for size-dependent residual variance (Fig. 7A), show clear signals of negative skew and positive excess kurtosis across most of the size distribution but strongest in the middle of the size distribution (Fig. 7B).

To better capture size transitions, we need a distribution with negative skew and positive excess kurtosis, but both of which may be negligible at some sizes. We first tried Johnson's S_U and then the skewed t distributions, both of which are limited to positive excess kurtosis. Both distributions provided some improvement over the Gaussian, but were not happy with the fit of either. Iterating through the workflow (Fig. 1), we arrived, again, at the SHASH distribution, which is more flexible than either the JSU or skewed t , capable of capturing a greater range of kurtosis for a given amount of skew, and vice versa (Steve's NPSkewKurtosisRanges.pdf). Furthermore, fitting the SHASH as a generalized additive model with `mgcv` allowed for flexible, non-monotonic size-dependence in skewness and kurtosis without the need for model selection on specific size-dependent functions; through iterations of trial and error, we found this flexibility was necessary to generate simulated data that compared favorably to the real data. The other distributions that we tried are not available as `mgcv` families, so we fit these with

415 custom maximum likelihood functions, an approach we illustrate in the next case study.
 416 The final growth model was similar to the SHASH gam in the coral case study, but
 417 with random intercepts for the location parameter, representing spatial and temporal
 418 heterogeneity:

```

419 fit_shash <- gam(list(logvol_t1 ~ s(logvol_t,k=4) +
420   s(plot,bs="re") + s(year_t,bs="re"), # location
421   ~ s(logvol_t,k=4), # log-scale
422   ~ s(logvol_t,k=4), # skewness
423   ~ s(logvol_t,k=4)), # log-kurtosis
424   data = CYIM_grow,
425   family = shash,
426   optimizer = "efs")
  
```

427 The final SHASH model provided good correspondence between simulated and
 428 real data, and provided more compelling improvement over the Gaussian model than
 429 we saw in the coral case study (Fig. 8). The SHASH model over-estimated negative
 430 skew at some sizes relative to the signal of skewness in the data (Fig. 8C), but the nature
 431 of size-dependent skew in the data is not very biologically plausible and may instead
 432 be driven by the tail-wagging tendency of gams. As in the coral case study, we see
 433 that correctly modeling skewness and kurtosis improved estimation of the mean and
 434 standard deviation (Fig. 8A,B), yielding a growth model that is clearly truer to the data
 435 than the pilot Gaussian fit.

436 We explored how improved growth modeling influenced IPM results, leveraging
 437 the plot and year structure of the study design to quantify spatial and temporal vari-
 438 ance in fitness. We used the fitted random effects from the vital rate models to estimate
 439 the asymptotic growth rate for each year (λ_t), centered on the average plot, and for
 440 each plot (λ_p), centered on the average year. This allowed us to quantify demographic
 441 variance associated with temporal and spatial heterogeneity. We found that the Gaus-
 442 sian growth model tended to over-estimate λ_t , particularly in the harshest years (Fig.
 443 9A), and thus under-estimated temporal variance in fitness ($Var(\lambda_{t(Gaussian)}) = 0.0018$,
 444 $Var(\lambda_{t(SHASH)}) = 0.0023$). The opposite was true for plot-to-plot variation (Fig. 9B),
 445 where the Gaussian model under-estimated λ_p and over-estimated spatial variance in
 446 fitness ($Var(\lambda_{p(Gaussian)}) = 0.00015$, $Var(\lambda_{p(SHASH)}) = 0.000088$). Across both growth
 447 models, fluctuations in fitness were stronger through time than across space. The
 448 difference in temporal variance would suggest that Gaussian growth modeling would
 449 lead to over-estimation of the stochastic growth rate λ_S , since temporal variance has

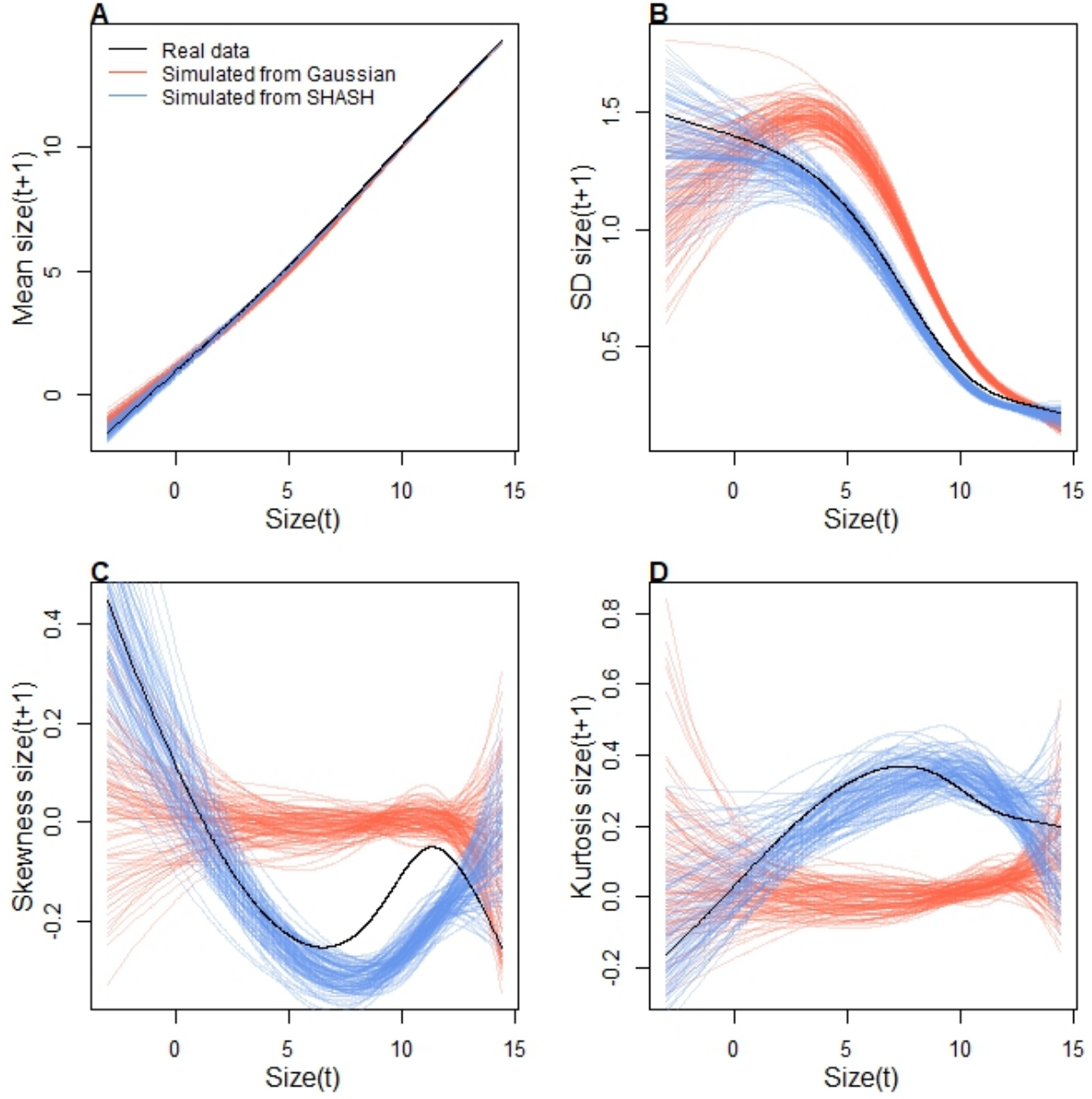


Figure 8: Comparisons among real cactus data and data simulated from Gaussian and SHASH growth models for mean, standard deviation, NP skewness, and NP excess kurtosis of future size conditional on current size. Figure made by script `cactus_growth_modeling_qgam.R`.

a negative influence on λ_S . However, this was not the case: stochastic IPMs based on Gaussian and SHASH growth models had nearly identical stochastic growth rates ($\lambda_S(\text{Gaussian}) = 0.9906$, $\lambda_S(\text{SHASH}) = 0.9909$). This is likely because temporal fluctuations in vital rates, which is where the SHASH growth model would make a difference, have a weaker influence on λ_S than the temporal fluctuations in size structure that they

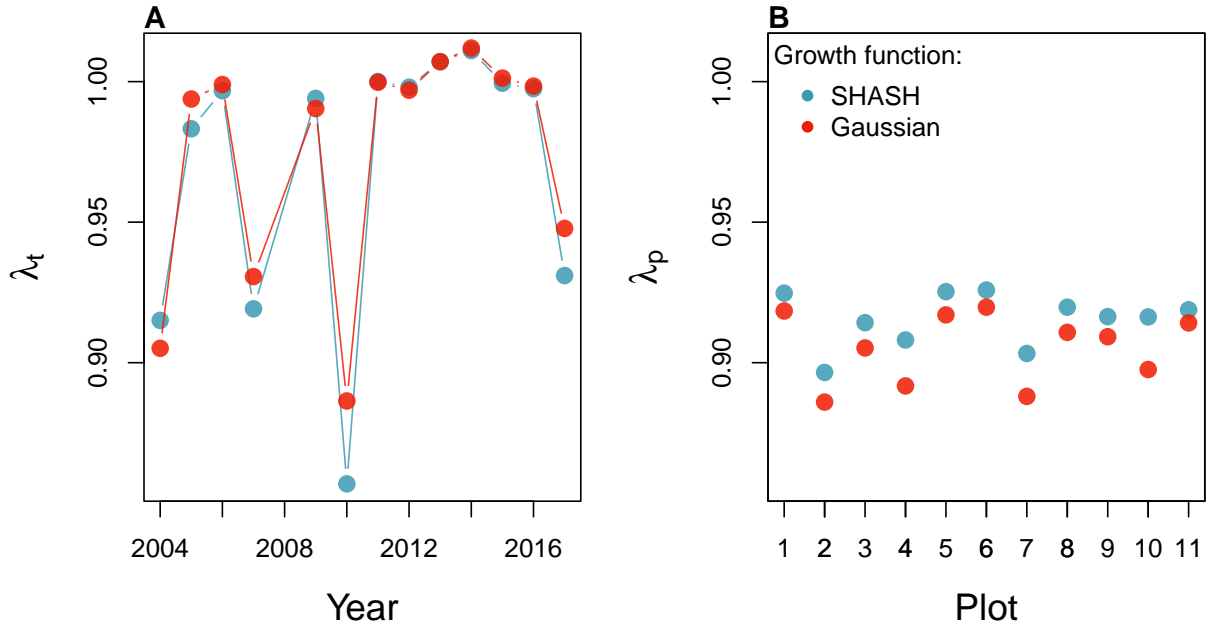


Figure 9: Temporal (A) and spatial (B) heterogeneity in fitness for the tree cholla cactus (*Cylindriopuntia imbricata*) predicted by IPMs using Gaussian or SHASH growth models. Figure made by script `cactus_growth_modeling_qgam.R`.

455 generate (Compagnoni et al., 2016; Ellis and Crone, 2013). Thus, depending on the target
 456 of one's analysis, modeling non-Gaussian size transitions with a Gaussian growth model
 457 could bias results in either direction, or make no difference at all.

458 4 Case study: creosotebush, *Larrea tridentata*

459 Our next case study comes from our studies of the woody shrub creosotebush (*Larrea tri-
 460 dentata*) at the Sevilleta Long-Term Ecological Research (LTER) site in central New Mex-
 461 ico, US. At this site as elsewhere in the Southwest US, creosotebush is encroaching into
 462 desert grassland habitats. The data described here were collected along transects span-
 463 ning grass-shrub ecotones to understand patterns of density dependence in creosotebush
 464 demography. Specifically, we asked whether fitness is maximized approaching zero den-
 465 sity at the leading edge of the expansion front (consistent with ‘pulled’ expansion), or
 466 whether there is a demographic advantage for shrubs at higher density due to positive
 467 feedbacks expected for ecosystem engineers (leading to ‘pushed’ expansion). Our pub-
 468 lished study (Drees et al., 2023) used a spatial integral projection model (SIPM) to predict
 469 the speed of shrub encroachment, assuming normally-distributed size transitions. Here
 470 we step through our suggested workflow to ask whether a non-Gaussian model would
 471 have been more faithful to the data, and how such an improvement would influence

472 predictions for the speed of encroachment. We use this case study to illustrate several
473 new elements and challenges, including modeling skewness and kurtosis as functions of
474 expected future size (instead of initial size) and using distributions that are not available
475 as **mgcv** families. In fact, to diversify our use of software and illustrate alternatives, we
476 do not use **gam**'s for any element of this case study.

477 Growth data come from 522 shrubs censused longitudinally over four years (2013–
478 2017). Census individuals occurred along 12 replicate transects (200 to 600 m in length)
479 that spanned gradients of shrub density along shrub-grass ecotones. Size was measured
480 as volume of an elliptical cone based on height and width measurements; the size vari-
481 able of the IPM was the natural logarithm of volume (cm^3). For each census individual,
482 we recorded the size and density of all conspecifics within the five-meter transect “win-
483 dow” in which it occurred, and took the sum of all sizes within the window as a measure
484 of local density. The data are available in Ochocki et al. (2023).

485 As an initial Gaussian approach, we first fit a set of candidate linear mixed mod-
486 els, including transect as a random effect, that represented competing hypotheses for
487 how size, density, and their interaction influence growth. Specifically, we fit five can-
488 didate Gaussian models that included fixed effects of initial size only (model 1), size
489 and density (model 2), and size, density, and their interaction (model 3), allowing for
490 shrubs of different sizes to have different growth responses to local density. Models 4
491 and 5 mirrored models 2 and 3 but included second-order terms for density, allowing
492 for the possibility of non-monotonic density dependence. As in (Drees et al., 2023) we
493 pooled data across three transition years. Initial AIC rankings of these pilot models fa-
494 vor model 4 slightly over model 5 ($\Delta AIC = 0.8$) and significantly over all other models
495 ($\Delta AIC > 2$). However, these models were fit assuming constant variance, and inspection
496 of the residuals of the best model indicate this is not a safe assumption.

497 Unlike our previous case studies, here we have multiple fixed effects that may influ-
498 ence the variance of future size. In cases such as this, we recommend modeling variance
499 as a function of expected future size, rather than initial size as we did with the corals
500 and cacti. The expected (or “fitted”) values reflect the combined influence of all fixed
501 and random effects, and therefore implicitly account for multiple sources of variation in
502 the variance. While there are several convenient software packages for simultaneously
503 modeling Gaussian mean and variance as functions of independent variables (**mgcv** for
504 **gam** models as we saw above, **nlme** for linear models), **modeling variance as a function**
505 **of the mean is trickier because they cannot easily be fit simultaneously**². Here we us an
506 iterative re-weighting approach – which is not elegant, but it works. For Gaussian mod-

2 After I wrote this I discovered that **nlme** can fit residual variance as a function of **fitted(.)**.

507 els, weights w_i can be used to indicate that the observations y_i vary in their dispersion
 508 around the mean. In general, the iterative steps are:

1. Fit the expected value and normally-distributed residuals with constant variance:

$$y_i = \mu_i + \epsilon_i$$

$$\epsilon_i \sim N(0, \sigma)$$

2. Fit the standard deviation of the residuals as a function of the expected value.

Weights are derived as the inverse of the fitted variance:

$$\epsilon_i \sim N(0, f(\mu_i))$$

$$w_i = 1/f(\mu_i)^2$$

3. Re-fit the observation model, weighting the residual variance according to step 2:

$$y_i = \mu_i + \epsilon_i$$

$$\epsilon_i \sim N(0, \sigma \times \sqrt{w_i})$$

509 We iterated steps 2 and 3 until the weights did not change. In step 2, we modeled
 510 the standard deviation as a simple linear function of the expected value ($\log(f(\mu_i)) =$
 511 $\beta_0 + \beta_1 * \mu_i$) but other functions are possible, as is model selection among them. We
 512 did this for all candidate models and, for fair AIC comparison, we re-fit all candidate
 513 models with the same weights, estimated from the top model. The updated model
 514 selection continued to favor model 4, but now with a stronger improvement over the
 515 next-best model ($\Delta AIC = 3.0$).

516 The resulting Gaussian growth model predicts strong initial size-dependence and
 517 weak and slightly nonlinear (but monotonic) negative density dependence (Fig. 10A).
 518 The model accounts for non-constant variance through the fitted weights, which in-
 519 dicate greater dispersion for smaller values of expected size ($\beta_1 = -0.21$; Fig. 10B).
 520 mostly Quantiles of the standardized residuals indicate size-dependent mostly negative
 521 skew and positive excess kurtosis, especially at smaller expected sizes (Fig. 10C).³ As

³Note that there is still a variance trend in the standardized residuals—rather unsatisfying! I have been through this backwards and forwards and my take is that this is a product of the sample size imbalance between small and large plants. The quantile regression is doing its best. SPE: I think a lot of it has to do with the fitted SD function. `gam(family="gaulss")` says the standard deviation flattens out near the bottom, and using that SD function there is a smaller (but still unsatisfying) variance trend in the standardized residuals.

522 a candidate for improvement, we turned to the Johnson's S_U (JSU) distribution, a four-
523 parameter, leptokurtic distribution capable of skew in either direction.

524 Following our suggested workflow, rather than re-fitting a JSU model from scratch,
525 we parameterize a model a model where the residuals from the Gaussian "pilot" model
526 are fitted by a JSU distribution. This relatively easy because the **gamlss.dist** package
527 provides a parameterization of the JSU in which the location parameter μ is the mean
528 and scale parameter σ is the standard deviation (Rigby et al., 2019). Using that, we
529 fitted the "hybrid" model by writing a likelihood function that uses the fitted mean and
530 standard deviation functions from Gaussian pilot model, and estimates the parameters
531 that control skewness and kurtosis as linear functions of predicted future size. The
532 "hybrid" likelihood looks like this [SPE: if we are going to use the spline SD function,](#)
533 [this will need to change:](#)

```
534 ## log_volume_t1 are the size obervations
535 ## GAU_fitted are the predicted future size from the best Gaussian model
536 ## pars is a vector of free parameters to be estimated
537 JSULogLik=function(pars){
538     dJSU(x=log_volume_t1,
539         mu=GAU_fitted,
540         sigma=exp(GAU_sd_coef[1]+GAU_sd_coef[2]*GAU_fitted),
541         nu = pars[1]+pars[2]*GAU_fitted,
542         tau = exp(pars[3]+pars[4]*GAU_fitted), log=TRUE)
543 }
```

544 The mean of the JSU is set to that of the best Gaussian model (`GAU_fitted`) and the
545 standard deviation is a function of the mean according to the coefficients (`GAU_sd_coef`)
546 estimated through iterative re-weighting. Based on diagnostics of the standardized resid-
547 uals (Fig. 10), JSU parameters that control skewness and kurtosis are defined as linear
548 functions of the mean, and those coefficients are estimated by maximum likelihood. This
549 approach relies on the robustness of Gaussian models fitted mean and variance to devia-
550 tions from normality. If one is skeptical of this approach, it is possible to simultaneously
551 re-fit all parameters of the JSU in a maximum likelihood framework. However, incorpo-
552 rating random effects into a custom likelihood model is non-trivial (we provide guidance
553 on one way to do this, using the "shrinkage" approach, in Appendix XX). Therefore a
554 key advantage of the hybrid approach is convenient retention of the fitted random ef-
555 fects and associated variance components, which get shuttled from the Gaussian model
556 into the non-Gaussian model without any fuss (it was critical that we used a parameter-

ization of the JSU for which `mu` is the mean and `sigma` is the standard deviation). And, if this approach does not “work” (i.e., deviations from normality biased the fitted values of the Gaussian model) one would quickly find out through the simulation step of the workflow. In this case, the hybrid JSU model performed well, generating simulated data that aligned with the real data better than the best Gaussian model, particularly in **standard deviation⁴** and kurtosis (Fig. 11). The JSU model has exactly the same mean and standard deviation of future size as the Gaussian, but Fig. 10 uses the quantile-based nonparametric mean and standard deviation. The results show that even though the JSU was not fitted to match those, it comes closer than the Gaussian model as a result of accounting for the skew and kurtosis.

The improvement of the JSU over the Gaussian growth model, while visually satisfying, had virtually no influence on SIPM results. Models using Gaussian or JSU growth kernels had nearly identical, monotonic decreases in λ with increasing local density, and nearly identical wave velocities (Fig. 12). This species has very low mortality risk once established (mean remaining life expectancy of a median-sized shrub is 24,408 years) and its population growth and wave expansion are limited by very low seedling recruitment ((Drees et al., 2023)). Weak size-dependence in survival likely explains why the improvement in growth modeling had little influence on SIPM predictions.

⁴I am a little mystified as to why the JSU is so much better. It is literally the same SD in both distributions. SPE: it's the same SD but not the same quantile-based nonparametric SD, and the JSU gets the nonparametric SD better. With the curves offset, you can see that in also does better at the NP mean.

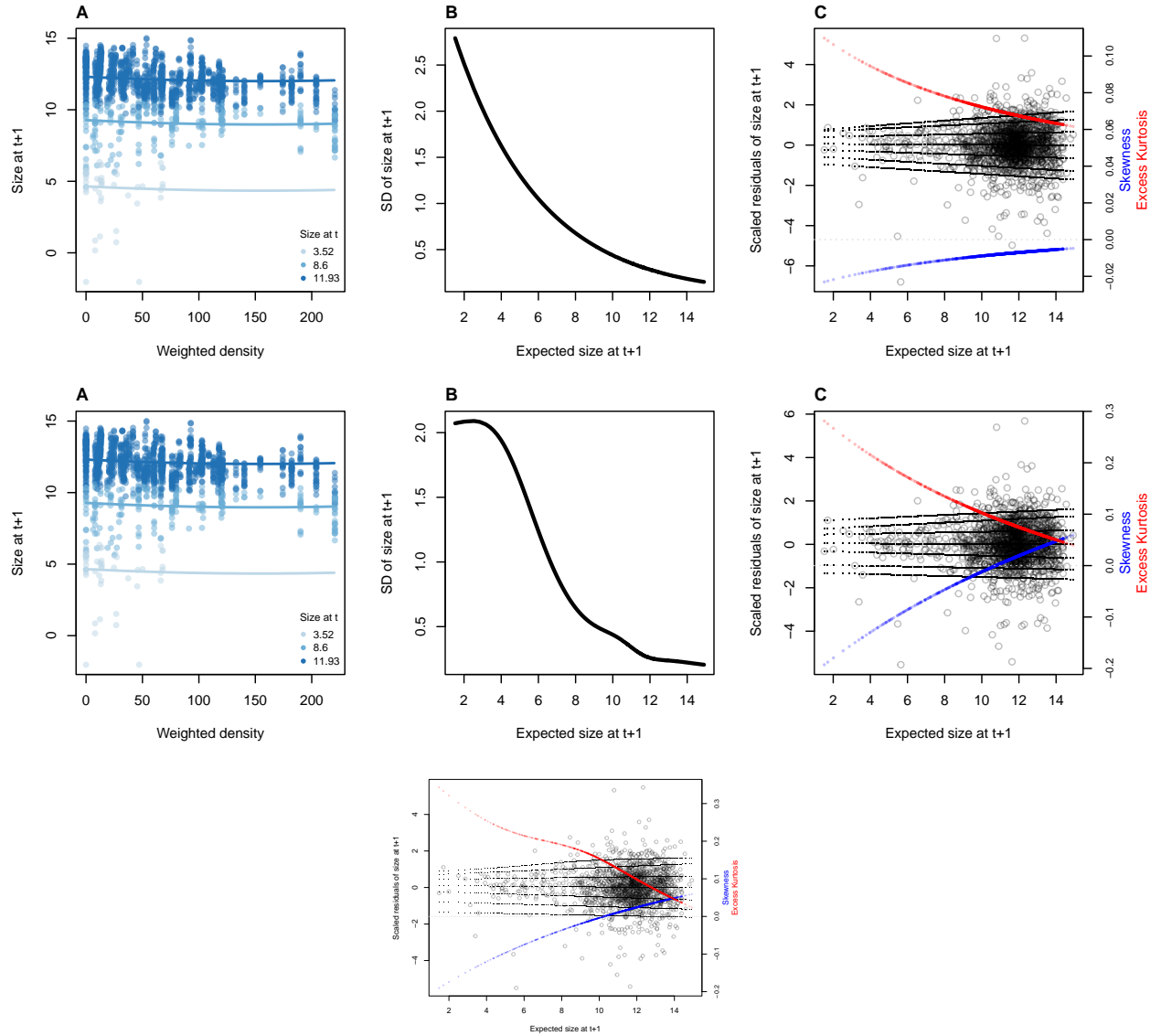


Figure 10: Two and 1/3 versions of the same figure. TOP, lmer growth model with log-linear model for SD as a function of fitted. MIDDLE, lmer growth model with spline SD as a function of fitted using gaulss, quantiles from rq (parametric). Bottom: rightmost panel redrawn with spline model for growth and SD using gaulss, and qgam fitting of residual quantiles. **A**, Creosotebush size transition data with respect to initial size (colors) and local weighted density (sum of sizes of all plants within a five-meter transect window). Size is quantified as the natural logarithm of plant volume (cm^3). **B**, Standard deviation of size at time $t + 1$ as a function of expected size at $t + 1$ (the fitted values), estimated by iterative re-weighting. **C**, Quantile regressions of scaled residuals on size and nonparametric estimates of skewness (blue) and excess kurtosis (red) derived from them. Black lines in **C** show the 5th, 10th, 25th, 50th, 75th, 90th, and 95th quantiles. All figures made by script `creosote_growth_modeling_rq.R`.

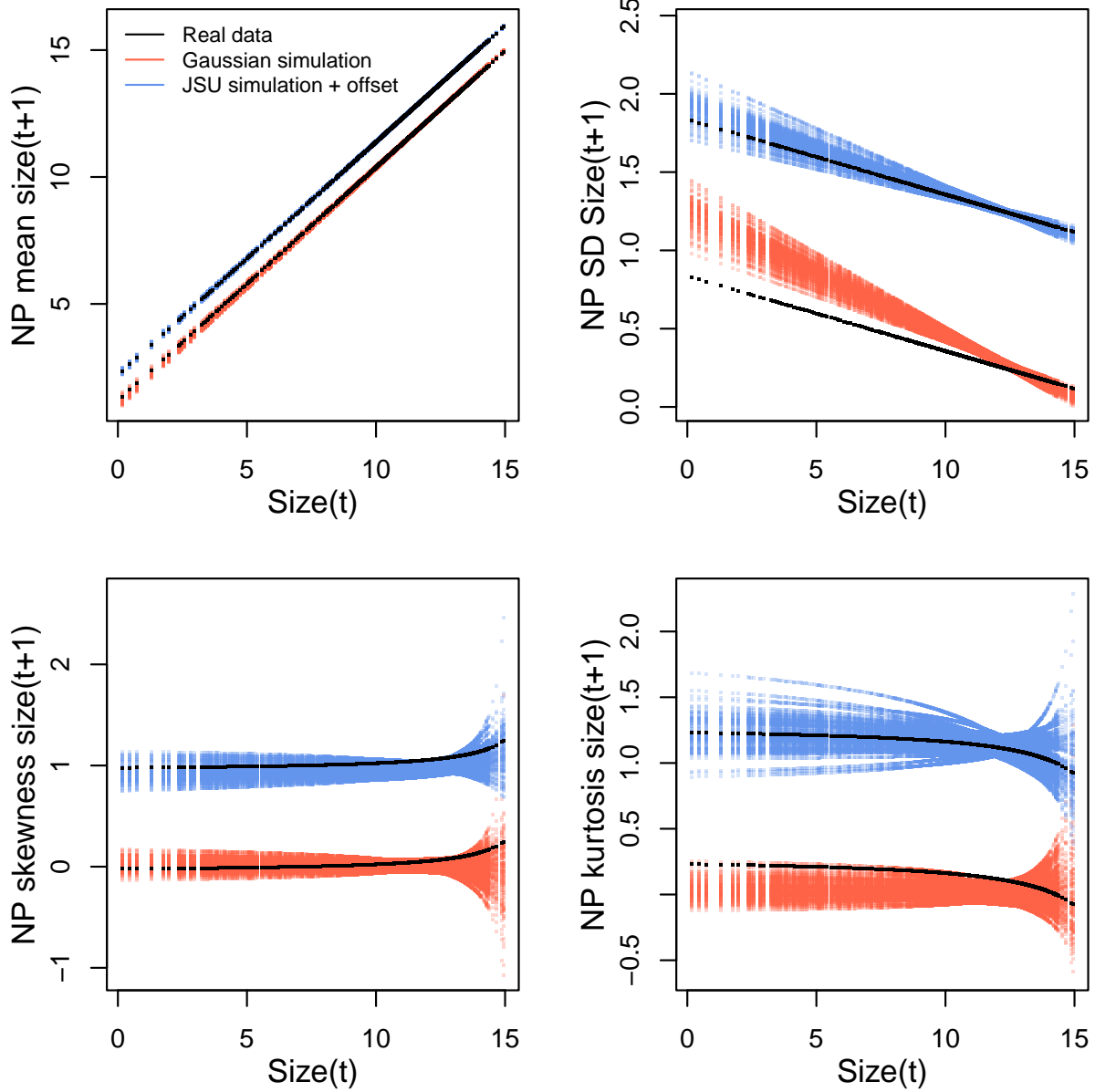


Figure 11: Comparisons between real creosotebush data and data simulated from Gaussian and JSU growth models for mean, standard deviation, NP skewness, and NP excess kurtosis of future size conditional on current size. Moments of the future size distribution are plotted with respect to initial size; their distribution is also conditional on density but initial size is by far the stronger predictor of future size, so we chose this visualization. Values for the JSU model (and the corresponding “real data” values) are offset vertically by one unit for comparison. Figure made by script `creosote_growth_modeling_qgam.R`.

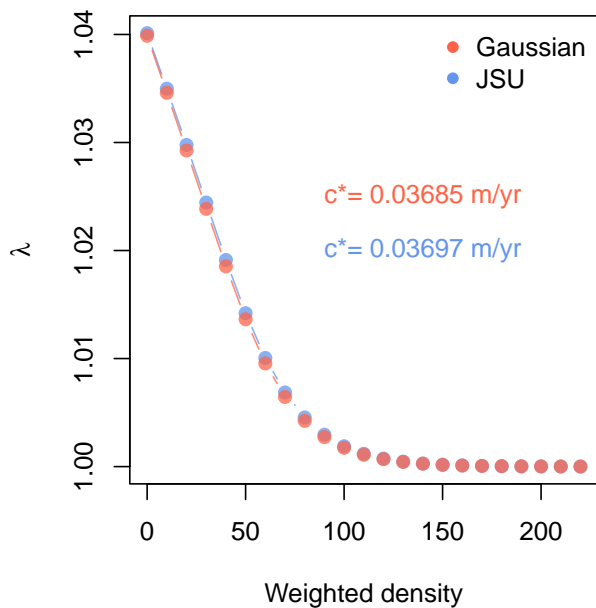


Figure 12: Density dependence in fitness (λ) and asymptotic velocity of the creosote encroachment wave (c^*) for Gaussian and JSU growth kernels. Weighted density is the sum of sizes ($\log(cm^3)$) of all conspecifics within a five-meter transect “window”. Figure made by script `creosote_growth_modeling_qgam.R`.

575

5 Case study: lady orchid, *Orchis purpurea*

576 Our final case study examines selection on life history strategies in the lady orchid *Or-*
577 *chis purpurea*. In a prior study, Miller et al. 2012 contrasted the growth trajectories from
578 year t to $t + 1$ for plants that did or did not flower in year t , as a way to quantify costs
579 of reproduction. The different growth kernels were then used in an IPM to quantify
580 evolutionarily stable life history strategies: the optimal flowering size that balances ben-
581 efits of flowering at larger sizes against the risk of dying before reaching those sizes.
582 The original study assumed a Gaussian distribution of size transitions and allowed for
583 non-constant variance with respect to initial size. Here we re-visit that analysis applying
584 our growth modeling workflow to derive improved growth kernels for flowering and
585 non-flowering orchids.

586 The data, originated by Dr. Hans Jacquemyn and used here with permission, come
587 from 368 plants in a Belgian population that was censused annually from 2003 through
588 2011 (for this reanalysis we are using data only from the “light” habitat). Size was mea-
589 sured as leaf area (cm^3) summed over all leaves, and we analyzed the natural logarithm
590 of total leaf area as the size variable of the IPM.

591 As a pilot Gaussian approach, we fit six candidate models in which the mean was
592 a function of initial size only, additive effects of initial size and flowering status, and
593 interaction between size and flowering, and the standard deviation was a function of
594 size only (models 1-3) or size and flowering status (models 4-6). All models included a
595 random intercept for year. As another variation on software and an alternative to two-
596 step fitting or iterative re-weighting, here we use `nlme::lme()`, which can simultaneously
597 fit linear predictors for mean and variance. For example, model 1 was:

```
598 orchid_GAU[[1]]<-lme(log_area_t1~ log_area_t,  
599 weights=varExp(form=~ log_area_t),  
600 random=~ 1|begin.year,data=orchid_grow,method="ML")
```

601 Model 3 (size \times flowering) was strongly favored, consistent with prior results that non-
602 flowering plants have a growth advantage over flowering plants. Growth variance de-
603 clined with initial size for both reproductive classes (Fig. 13A-B) and skewness and kur-
604 tosis of the standardized residuals indicate strong deviations from normality (Fig. 13C-
605 D). For most sizes, left skew and excess kurtosis were more severe for non-reproductive
606 plants, with tail imbalance ca. 10% of their total and tail weights 10–20% fatter than
607 Gaussian.

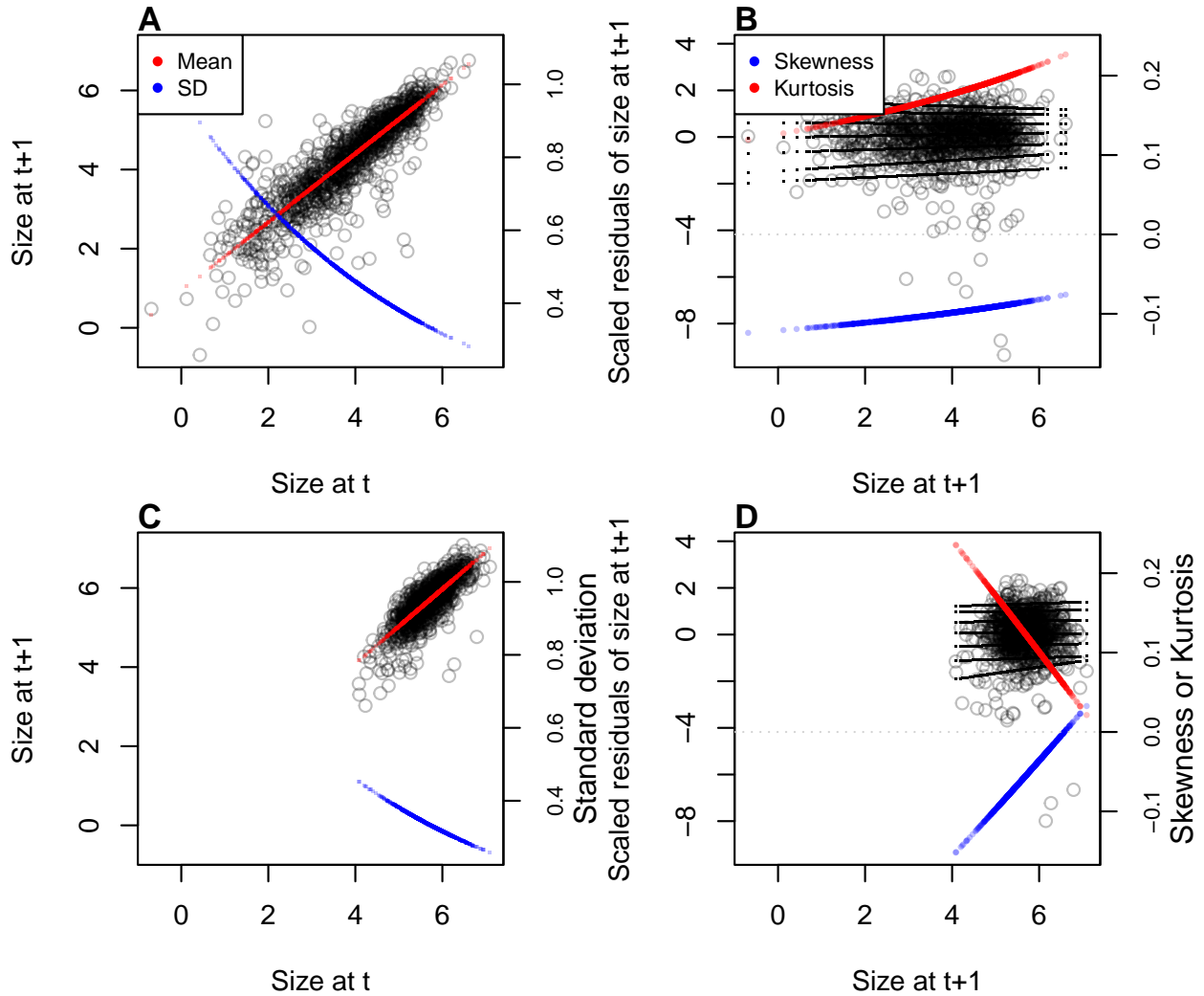


Figure 13

As improvements, we explored the skewed t and Johnson's SU distributions, both leptokurtic distributions with flexible skewness. We were happier with the skewed t , which we fit in a similar way as we fit the JSU to the creosote data, setting the mean and standard deviation to the Gaussian fits and estimating free parameters controlling skewness and kurtosis:

```

608     ## log_area_t1 and log_area_t are the size obervations
609     ## flowering indicates reproductive status at time t (0 or 1)
610     ## GAU_fitted and GAU_sd are mean and standard deviation from lme
611     ## pars is a vector of free parameters to be estimated
612     SSTLogLik=function(pars){
613       dSST(x=log_area_t1,
614             log_area_t=mean(log_area_t),
615             sd=log_area_t*GAU_sd,
616             pars=pars)
617   }

```

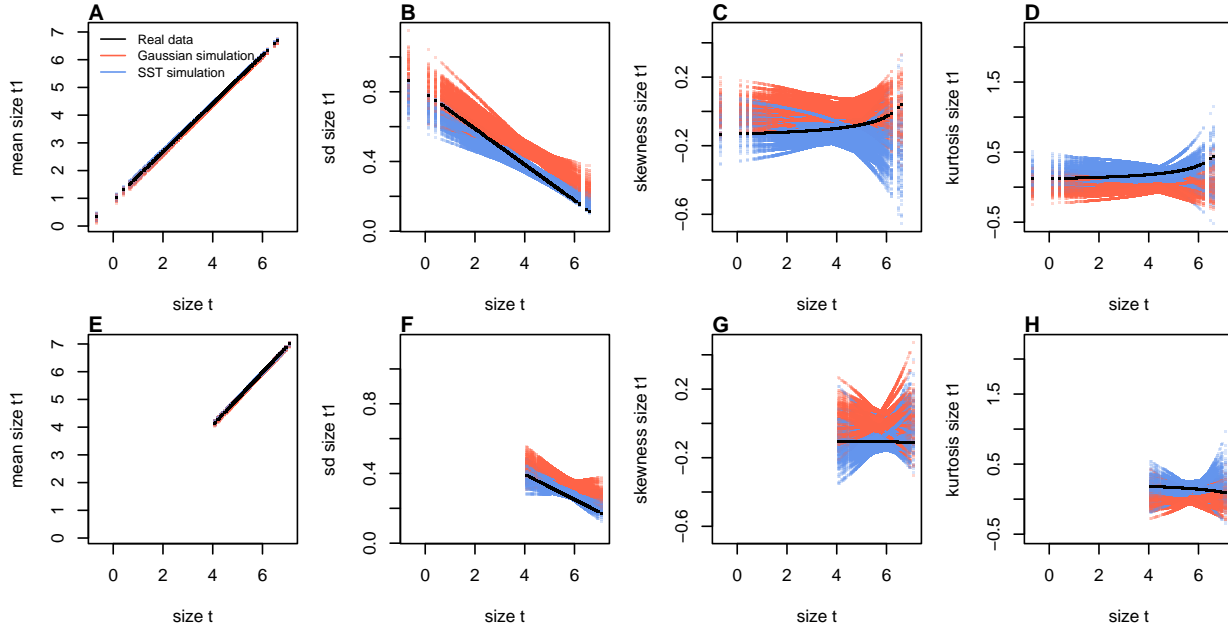


Figure 14: Comparisons between real orchid data and data simulated from Gaussian and skewed t growth models for mean, standard deviation, NP skewness, and NP kurtosis of future size conditional on current size. Top row (A-D) shows plants that were vegetative at the start of the transition year and bottom row (E-H) shows plants that were flowering at the start of the transition year. Figure made by script `orchid_growth_modeling_rq.R`.

```

619     mu=GAU_fitted,
620     sigma=GAU_sd,
621     nu = exp(pars[1] + pars[2]*log_area_t + pars[3]*as.logical(flowering) + pars[4]
622     tau = exp(pars[5] + pars[6]*log_area_t + pars[7]*as.logical(flowering) + pars[8]
623     log=TRUE)
624   }

```

625 `gamlss.dist:dSST` is a parameterization of the skewed t in which `mu` and `sigma` are the
626 mean and standard deviation, respectively. Based on diagnostics of the standardized
627 residuals (Fig. 13) we allowed `nu` and `tau` to vary by size and differ between flowering
628 and non-flowering plants (note that the `tau` parameter uses a $\log(x - 2)$ link function).
629 Size transition data simulated from this model corresponded favorably to the real data,
630 much better than the pilot Gaussian model, including improvements in the **standard**
631 **deviation**⁵, skewness, and kurtosis of future size (Fig. 14).

632 Finally, we used the improved growth model to revisit key results of the original
633 study. Miller et al. (2012) used the orchid IPM to estimate the evolutionarily stable strat-

⁵Again, the improvement here is surprising to me and I am unsure what to say about it. SPE: again, it's probably about the "usual" mean and SD versus the quantile-based NP versions.

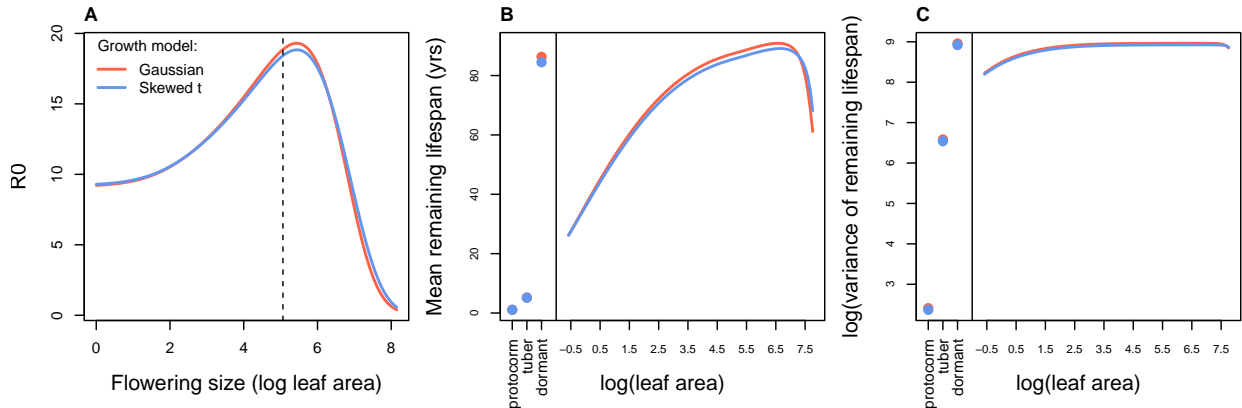


Figure 15: Orchid life history results from IPMs using Gaussian or skewed t growth models. **A**, Lifetime reproductive success (R_0) as a function of mean size of flowering. Dashed vertical line shows the observed mean flowering size. **B-C**, Mean and variance of remaining lifespan as a function of size or stage. The orchid IPM includes three discrete below-ground stages (protocorm, tuber, and dormant plant) in addition to continuous size of above-ground plants. **SPE: the variance of lifespan results are now correct, using Chrissy Hernandez's functions instead of RAGE. And the result is, non-Gaussian again has no effect.**

634 egy (ESS) as the mean size at flowering that maximizes lifetime reproductive success
 635 (R_0), given the constraint that flowering when small reduces growth and thus elevates
 636 mortality risk. Repeating that analysis here, we found that improved growth modeling
 637 has virtually no influence on predictions for optimal life history strategies (Fig. 15). ESS
 638 flowering sizes were nearly identical between IPMs with Gaussian vs skewed t growth
 639 models, and both aligned well with the observed mean flowering size (dashed vertical
 640 line in Fig. 15A). Extending beyond the original study, we also explored expected re-
 641 maining lifespan for different ages and sizes (R package **Rage** (Jones et al., 2022)). Gaus-
 642 sian and skewed t growth models predicted nearly identical mean remaining lifespans
 643 across the stage and size distribution (Fig. 15B). **However, the skewed t model predicted**
 644 **consistently greater variance in remaining lifespan, nearly 10% greater at some sizes.⁶**
 645 Thus, as we have seen in other case studies, the practical consequences of improved
 646 growth modeling depend on what one aims to learn from the IPM.

⁶*Do not believe this result! I have left it here as a placeholder because I would like to do this correctly. But I think there are problems with Rage's `life_expect_var()` function. The predicted variance declines linearly with matrix dimension.*

6 Discussion

Much of the appeal of integral projection models has stemmed from their embrace of continuous size structure through reliance on regression-based approaches, and the potentially complex fixed- and random-effect structures that these approaches allow. Using familiar statistical tools and with relatively few parameters to estimate, IPM users can incorporate important sources of variation in demography and interrogate their influence on ecological and evolutionary dynamics. With this opportunity comes the burden of getting it right: IPMs are good models of the populations they are intended represented only insofar as the statistical models provide good fits to the underlying data. The growth sub-model is the trickiest part of “getting it right” because it defines a distribution of future size conditional on current size. Distributions have many properties – “moments” – and a good growth model should recapitulate the properties of real size transitions. The default assumption of normally distributed size transitions, employed overwhelmingly across 20+ years of IPM studies, is an arbitrary historical precedent. In four case studies (chosen simply because we had the data at our fingertips) and, we suspect, more broadly, skewness and excess kurtosis were common features of size transition data: shrinking was more common than growing, and large changes in size were more common than a Gaussian model would predict. Our most important message is that the standard assumption of normally-distributed size transitions should be abandoned and a more inquisitive process of growth modeling should take its place.

We have attempted to lay out a general workflow for what that process should look like, guided by visual diagnostics of standardized residuals. One implication of relying on visual diagnostics is that goodness of fit is in the eye of the beholder. This approach can empower IPM users to make informed choices, but it is not very prescriptive: we have not suggested any hard rules for when one or another distribution should be used, only that a good growth model should generate data that look like the real thing. Alternatively, model selection could be used to identify best-fitting growth distributions and best-fitting functions for higher moments. However, model selection among growth distributions with 3-5 parameters, each of which may be functions of state variables or fitted values, can quickly explode in complexity, and we are not convinced it is worth the trouble. It is possible to find a good growth model without worrying about which one is “best”.

In all of our case studies, non-Gaussian growth models always yielded more satisfying fits to size transition data than the Gaussian models published in those papers. However, much to our relief, none of these re-analyses yielded a “gotcha” result that

682 overturned results of the original study. In this small sampling of case studies, im-
683 proved growth modeling had only modest effects on IPM results. We caution against
684 taking too much comfort in this outcome; we can imagine other scenarios in which the
685 choice of the growth distribution could be more consequential. It is worth noting that
686 three of our case studies focused on perennial plants and the fourth focused on corals,
687 which are demographically similar to perennial plants (heavy losses during recruitment
688 but high survival once established). Life cycles such as these may be relatively robust to
689 subtle features of the growth kernel. More systematic comparative analyses across may
690 provide insight into which types of species and life histories are more likely to exhibit
691 strong skewness and kurtosis of size transitions, and the conditions under which demo-
692 graphic analysis is more or less sensitive to these features of size transition. It is also
693 worth noting, as we saw in several case studies, that different outputs from the same
694 model can be more or less sensitive to the choice of growth distribution.

695 Some issues to be discussed.

- 696 • Many software options: lme4/maxLik, mgcv, rstan
- 697 • Comparison of our approach with beta regression method.
- 698 • We have emphasize growth but same principles apply to other continuous state
699 transitions, eg disease IPMs.
- 700 • Eviction still a problem for unbounded distributions.

701 Acknowledgements

702 This research was supported by US NSF grants DEB-1933497 to SPE and DEB-1754468,
703 2208857, and 2225027 to TEXM.

704 7 Authorship statement

705 All authors discussed all aspects of the research and contributed to developing methods,
706 analyzing data, and writing and revising the paper.

707 8 Data accessibility statement

708 No original data appear in this paper. Should the paper be accepted, all computer scripts
709 supporting the results will be archived in a Zenodo package, with the DOI included at

⁷¹⁰ the end of the article. During peer review, our data and code are available at https://github.com/texmiller/IPM_size_transitions.
⁷¹¹

712 **Literature Cited**

- 713 Anscombe, F. J. and Glynn, W. J. (1983). Distribution of the kurtosis statistic b_2 for
714 normal samples. *Biometrika*, 70(1):227–234.
- 715 Bates, D., Sarkar, D., Bates, M. D., and Matrix, L. (2007). The lme4 package. *R package
716 version*, 2(1):74.
- 717 Bruno, J. F., Ellner, S. P., Vu, I., Kim, K., and Harvell, C. D. (2011). Impacts of aspergillosis
718 on sea fan coral demography: modeling a moving target. *Ecological Monographs*,
719 81(1):123–139.
- 720 Compagnoni, A., Bibian, A. J., Ochocki, B. M., Rogers, H. S., Schultz, E. L., Sneck, M. E.,
721 Elderd, B. D., Iler, A. M., Inouye, D. W., Jacquemyn, H., et al. (2016). The effect of
722 demographic correlations on the stochastic population dynamics of perennial plants.
723 *Ecological Monographs*, 86(4):480–494.
- 724 Conn, P. B., Johnson, D. S., Williams, P. J., Melin, S. R., and Hooten, M. B. (2018). A guide
725 to bayesian model checking for ecologists. *Ecological Monographs*, 88(4):526–542.
- 726 Cooch, E. G. and White, G. C. (2020, accessed 5/17/2020). *Program MARK - a 'gentle
727 introduction'*. Available at phidot.org.
- 728 Coulson, T. (2012). Integral projections models, their construction and use in posing
729 hypotheses in ecology. *Oikos*, 121(9):1337–1350.
- 730 Crone, E. E. (2016). Contrasting effects of spatial heterogeneity and environmental
731 stochasticity on population dynamics of a perennial wildflower. *Journal of Ecology*,
732 104(2):281–291.
- 733 Czachura, K. and Miller, T. E. (2020). Demographic back-casting reveals that subtle
734 dimensions of climate change have strong effects on population viability. *Journal of
735 Ecology*.
- 736 D'Agostino, R. B. (1970). Transformation to normality of the null distribution of g_1 .
737 *Biometrika*, pages 679–681.
- 738 Davis, C. (2015). *sgt: Skewed Generalized T Distribution Tree*. R package version 2.0.
- 739 Drees, T., Ochocki, B. M., Collins, S. L., and Miller, T. E. (2023). Demography and
740 dispersal at a grass-shrub ecotone: a spatial integral projection model for woody plant
741 encroachment. *Ecological Monographs*, page e1574.

- ⁷⁴² Easterling, M. R., Ellner, S. P., and Dixon, P. M. (2000). Size-specific sensitivity: applying
⁷⁴³ a new structured population model. *Ecology*, 81(3):694–708.
- ⁷⁴⁴ Elderd, B. D. and Miller, T. E. (2016). Quantifying demographic uncertainty: Bayesian
⁷⁴⁵ methods for integral projection models. *Ecological Monographs*, 86(1):125–144.
- ⁷⁴⁶ Ellis, M. M. and Crone, E. E. (2013). The role of transient dynamics in stochastic popula-
⁷⁴⁷ tion growth for nine perennial plants. *Ecology*, 94(8):1681–1686.
- ⁷⁴⁸ Ellner, S. P., Adler, P. B., Childs, D. Z., Hooker, G., Miller, T. E., and Rees, M. (2022).
⁷⁴⁹ A critical comparison of integral projection and matrix projection models for demo-
⁷⁵⁰ graphic analysis: Comment. *Ecology*, 103(10):e3605.
- ⁷⁵¹ Ellner, S. P., Childs, D. Z., and Rees, M. (2016). *Data-driven Modeling of Structured Popula-
tions: A Practical Guide to the Integral Projection Model*. Springer, New York.
- ⁷⁵³ Gould, W. R. and Nichols, J. D. (1998). Estimation of temporal variability of survival in
⁷⁵⁴ animal populations. *Ecology*, 79:2531 – 2538.
- ⁷⁵⁵ Gu, C. (2013). *Smoothing Spline ANOVA Models*. Springer Science+Business Media, New
⁷⁵⁶ York, 2 edition.
- ⁷⁵⁷ Hadfield, J. D. et al. (2010). Mcmc methods for multi-response generalized linear mixed
⁷⁵⁸ models: the mcmcglmm r package. *Journal of Statistical Software*, 33(2):1–22.
- ⁷⁵⁹ Héault, B., Bachelot, B., Poorter, L., Rossi, V., Bongers, F., Chave, J., Paine, C. T., Wagner,
⁷⁶⁰ F., and Baraloto, C. (2011). Functional traits shape ontogenetic growth trajectories of
⁷⁶¹ rain forest tree species. *Journal of ecology*, 99(6):1431–1440.
- ⁷⁶² Jones, M. and Pewsey, A. (2009). Sinh-arcsinh distributions. *Biometrika*, 96:761 – 780.
- ⁷⁶³ Jones, M. C., Rosco, J. F., and Pewsey, A. (2011). Skewness-invariant measures of kurtosis.
⁷⁶⁴ *The American Statistician*, 65(2):89 – 95.
- ⁷⁶⁵ Jones, O. R., Barks, P., Stott, I., James, T. D., Levin, S., Petry, W. K., Capdevila, P., Che-
⁷⁶⁶ Castaldo, J., Jackson, J., Römer, G., et al. (2022). Rcompadre and rage—two r pack-
⁷⁶⁷ ages to facilitate the use of the compadre and comadre databases and calculation of
⁷⁶⁸ life-history traits from matrix population models. *Methods in Ecology and Evolution*,
⁷⁶⁹ 13(4):770–781.
- ⁷⁷⁰ Komsta, L. and Novomestky, F. (2015). Moments, cumulants, skewness, kurtosis and
⁷⁷¹ related tests. *R package version*, 14(1).

- 772 Link, W. A. and Nichols, J. D. (1994). On the importance of sampling variance to inves-
773 tigations of temporal variation in animal population size. *Oikos*, 69(3):539 – 544.
- 774 Louthan, A. M., Keighron, M., Kiekebusch, E., Cayton, H., Terando, A., and Morris, W. F.
775 (2022). Climate change weakens the impact of disturbance interval on the growth rate
776 of natural populations of venus flytrap. *Ecological Monographs*, 92(4):e1528.
- 777 McGillivray, H. (1986). Skewness and asymmetry: measures and orderings. *Annals of
778 Statistics*, 14:994–1011.
- 779 Metcalf, C. J. E., Ellner, S. P., Childs, D. Z., Salguero-Gómez, R., Merow, C., McMahon,
780 S. M., Jongejans, E., and Rees, M. (2015). Statistical modelling of annual variation for
781 inference on stochastic population dynamics using Integral Projection Models. *Methods
782 in Ecology and Evolution*, 6:1007–1017.
- 783 Miller, T. E. (2020). Long-term study of tree cholla demography in the los pinos
784 mountains, sevilleta national wildlife refuge. [https://doi.org/10.6073/pasta/
785 dd06df3f950afe4a4642306182237d13](https://doi.org/10.6073/pasta/dd06df3f950afe4a4642306182237d13).
- 786 Miller, T. E., Louda, S. M., Rose, K. A., and Eckberg, J. O. (2009). Impacts of insect
787 herbivory on cactus population dynamics: experimental demography across an envi-
788 ronmental gradient. *Ecological Monographs*, 79(1):155–172.
- 789 Miller, T. E., Williams, J. L., Jongejans, E., Brys, R., and Jacquemyn, H. (2012). Evolution-
790 ary demography of iteroparous plants: incorporating non-lethal costs of reproduction
791 into integral projection models. *Proceedings of the Royal Society B: Biological Sciences*,
792 279(1739):2831–2840.
- 793 Ochocki, B. M., Drees, T., and Miller, T. E. (2023). Density-dependent demography of
794 creosote bush (*larrea tridentata*) along grass-shrub ecotones. <https://doi.org/10.6073/pasta/ca53c16f16dcf9fb11f3ee99ea5445ac>.
- 796 Ohm, J. R. and Miller, T. E. (2014). Balancing anti-herbivore benefits and anti-pollinator
797 costs of defensive mutualists. *Ecology*, 95(10):2924–2935.
- 798 Ozgul, A., Childs, D. Z., Oli, M. K., Armitage, K. B., Blumstein, D. T., Olson, L. E., Tul-
799 japurkar, S., and Coulson, T. (2010). Coupled dynamics of body mass and population
800 growth in response to environmental change. *Nature*, 466(7305):482–485.

- 801 Peterson, M. L., Morris, W., Linares, C., and Doak, D. (2019). Improving structured
802 population models with more realistic representations of non-normal growth. *Methods*
803 in Ecology and Evolution, 10(9):1431–1444.
- 804 Plard, F., Schindler, S., Arlettaz, R., and Schaub, M. (2018). Sex-specific heterogeneity
805 in fixed morphological traits influences individual fitness in a monogamous bird
806 population. *The American Naturalist*, 191(1):106–119.
- 807 Rees, M., Childs, D. Z., and Ellner, S. P. (2014). Building integral projection models: a
808 user's guide. *Journal of Animal Ecology*, 83(3):528–545.
- 809 Rigby, R. A., Stasinopoulos, M. D., Heller, G. Z., and De Bastiani, F. (2019). *Distributions*
810 for modeling location, scale, and shape: Using GAMLSS in R. CRC press.
- 811 Salguero-Gómez, R. and Casper, B. B. (2010). Keeping plant shrinkage in the demo-
812 graphic loop. *Journal of Ecology*, 98(2):312–323.
- 813 Schielzeth, H., Dingemanse, N. J., Nakagawa, S., Westneat, D. F., Allegue, H., Teplitsky,
814 C., Réale, D., Dochtermann, N. A., Garamszegi, L. Z., and Araya-Ajoy, Y. G. (2020).
815 Robustness of linear mixed-effects models to violations of distributional assumptions.
816 *Methods in ecology and evolution*, 11(9):1141–1152.
- 817 Schultz, E. L., Eckberg, J. O., Berg, S. S., Louda, S. M., and Miller, T. E. (2017). Native
818 insect herbivory overwhelms context dependence to limit complex invasion dynamics
819 of exotic weeds. *Ecology letters*, 20(11):1374–1384.
- 820 Shriner, R. K., Cutler, K., and Doak, D. F. (2012). Comparative demography of an epi-
821 phytic lichen: support for general life history patterns and solutions to common prob-
822 lems in demographic parameter estimation. *Oecologia*, 170:137–146.
- 823 Stasinopoulos, D. M., Rigby, R. A., et al. (2007). Generalized additive models for location
824 scale and shape (gamlss) in r. *Journal of Statistical Software*, 23(7):1–46.
- 825 Stubberud, M. W., Vindenes, Y., Vøllestad, L. A., Winfield, I. J., Stenseth, N. C., and Lan-
826 gangen, Ø. (2019). Effects of size-and sex-selective harvesting: An integral projection
827 model approach. *Ecology and Evolution*, 9(22):12556–12570.
- 828 Wan, X., Wang, W., Liu, J., and Tong, T. (2014). Estimating the sample mean and stan-
829 dard deviation from the sample size, median, range and/or interquartile range. *BMC*
830 *medical research methodology*, 14:1–13.

- 831 Williams, J. L., Miller, T. E., and Ellner, S. P. (2012). Avoiding unintentional eviction from
832 integral projection models. *Ecology*, 93(9):2008–2014.
- 833 Wood, S. (2017). *Generalized Additive Models: An Introduction with R*. Chapman and
834 Hall/CRC, 2 edition.
- 835 Zhang, J. L. (2014). Comparative investigation of three bayesian p values. *Computational
836 Statistics & Data Analysis*, 79:277–291.

Appendices

S.1 The Jones-Pewsey distribution

Jones and Pewsey (2009) introduced a simple, tractable generalization of the Normal distribution with two additional parameters determining asymmetry (skewness), and tail weight (kurtosis) which can be either lighter or heavier than the Gaussian. It is defined as a transformation of a $\text{Normal}(0,1)$ random variable using the hyperbolic sine function (\sinh) and its inverse (asinh), as follows. The distribution family's base probability density $f_{\epsilon,\delta}$ is the probability density of the random variable $X_{\epsilon,\delta}$ where

$$Z = \sinh(\delta \text{ asinh}(X_{\epsilon,\delta}) - \epsilon) \quad (\text{S.1})$$

and Z has a $\text{Normal}(0,1)$ distribution. Equivalently,

$$X_{\epsilon,\delta} = \sinh\left(\frac{1}{\delta} \text{ asinh}(Z) + \frac{\epsilon}{\delta}\right). \quad (\text{S.2})$$

Parameters $\delta = 1, \epsilon = 0$ give the $\text{Normal}(0,1)$ distribution. Skewness has the sign of ϵ , and $\delta > 0$ controls tail weight, with heavier than Gaussian tails for $\delta < 1$ and lighter than Gaussian tails for $\delta > 1$. A formula for the density $f_{\epsilon,\delta}$ is given by Jones and Pewsey (2009, eqn. 2). The general four-parameter family with location parameter μ and scale parameter σ is defined as the probability densities of $\mu + \sigma X_{\epsilon,\delta}$. We refer to this as the JP distribution family.

As is unfortunately the case for most four-parameter distributions μ is not the mean, σ is not the standard deviation, ϵ is not the skew and δ is not the kurtosis. All else being equal, larger μ gives a larger mean, larger σ gives a higher standard deviation, higher ϵ gives higher asymmetry, and higher δ gives heavier tail weight. But each moment is jointly determined by all four parameters.

The main advantage of the JP distribution is that the attainable combinations of skewness and kurtosis are very broad, compared to other four-parameter families, and come very close to the theoretical limits on kurtosis as a function of skewness (Jones and Pewsey, 2009, Fig. 2). Additionally, being a transformation of the Normal makes it very simple to generate random numbers from the distribution, and to compute probability density, cumulative distribution, and quantile functions. There are also simple analytic formulas for the first four moments (Jones and Pewsey, 2009, p. 764) which we use below to define a centered and scaled version in which μ and σ are the mean and standard deviation.

867 The definition (S.2) shows that the distribution depends on ϵ only through the ratio
868 ϵ/δ . We have found that this property can be problematic for estimating distribution
869 parameters. Even with good sized ($n = 250$ or 500) data sets generated from the distri-
870 bution with known parameters, both maximum likelihood and Bayesian estimation were
871 unstable for some values of ϵ and δ , occasionally yielding estimates far from the truth.
872 One cause was a ridge in the (ϵ, δ) likelihood surface with a constant of ϵ/δ . Another is
873 that when δ is large, changes in ϵ have little effect.

874 To avoid that problems, we reparameterize the distribution as follows:

875
$$X_{\lambda, \tau} = \sinh(e^{-\tau} \operatorname{asinh}(Z) + \lambda). \quad (\text{S.3})$$

876 Thus, the two parameterizations are related by

877
$$\delta = e^\tau, \epsilon = \delta\lambda = e^\tau\lambda. \quad (\text{S.4})$$

878 The definition of τ allows it to take any real value, with negative values giving thinner
879 than Gaussian tails and positive values giving fatter than Gaussian tails. λ also can take
880 any real value, and the distribution's skew has the same sign as λ . Because the sinh
881 function is nonlinear, it is still the case that the skew depends on τ as well as λ , but the
882 "crosstalk" between the kurtosis and skew parameters is weaker. As a result, we found
883 that maximum likelihood estimation of parameter values was generally more reliable if
884 the distribution is parameterized in terms of τ and λ .

885 S.2 Estimating mixed-effects models using shrinkage

886 Ecologists often fit demographic and other statistical models that include random effects
887 terms to quantify variation among years, spatial locations, individuals, etc. Random
888 effects are a natural choice when interest centers on the magnitude of variation (e.g., how
889 much does mortality vary among years?) rather than individual values (e.g., mortality
890 in 2013). They also allow each estimate to "borrows strength" from others, so that (for
891 example) the estimate from a year with small sample size (and thus large sampling
892 variability) is shifted towards the center of the overall distribution.

893 Specialized software is often used to fit such models, such as the **nlme**, **lme4**, **mgcv**
894 and **gamm4** libraries in R, but these only allow a small subset of the distribution families
895 we want to consider for modeling growth increments (the **gamLss** package allows many
896 distribution families, but in our experience, even when random effects are simple in
897 structure the fitting algorithms often fail to converge or fail to find the global optimum).

898 One way past this limitation is Bayesian estimation, using STAN with user-written
899 (or borrowed) code for the chosen growth distribution (see section XX for an example).
900 In this appendix we describe another option, introduced by Link and Nichols (1994)
901 and Gould and Nichols (1998): fitting a fixed-effects model by Maximum Likelihood,
902 followed by shrinkage of coefficient estimates. None of the ideas here are original. The
903 material overlaps Appendix S1 of Metcalf et al. (2015), but for completeness we make
904 it self-contained. Appendix D of Cooch and White (2020) (written by K.D. Burnham)
905 provides more details and examples in the context of capture-recapture analysis.

906 Here we explain shrinkage using a simple model based on our analysis of *Pseu-*
907 *doroegneria spicata*. That model includes random effects for between-year variation in
908 the slope and intercept of future size (log area) as a function of initial size. To keep
909 the example simple, we assume that initial size and year are the only covariates, and
910 we assume that growth increments follow a skew-Normal distribution with noncon-
911 stant variance and constant skew parameter. Code for this example is in the script
912 `SimpleShrinkageExample.R`. The first part of the script generates an artificial data set
913 by fitting the model to a subset of the growth data (20th century Control plots), and
914 randomly generating new “size next year” values for each individual in the actual data
915 set. The second part contains the “data” analysis.

916 As in our *P. spicata* analysis, we assumed that that the skew and kurtosis parameters
917 were functions of the location parameter; this dominated ($\Delta AIC \approx 30$) the alternate
918 model with skew and kurtosis depending on initial size. The analogous Gaussian model,
919 with constant variance, could be fitted as follows using `lmer`:

920 `lmer(new.size ~ init.size + (init.size|year), data=growthData, REML=TRUE);`
921 where `growthData` is a data frame holding the data with year as an unordered factor.
922 For our skew-Normal model, we instead use maximum likelihood with all between-year
923 variation included as fixed effects. The appropriate design matrix is easily constructed
924 using the `model.matrix` function:

925 `U = model.matrix(~ year + init.size:year - 1, data=growthData)`

926 If there are T years, the matrix `U` specified in this way has $2T$ columns corresponding to
927 n annual intercepts and T annual slopes.

928 Using this design matrix, we can readily write a log likelihood function for use with
929 the `maxLik` package, with a log link function for the variance because it is necessarily
930 positive:

931 `LogLik=function(pars,new.size,U){`

```

932     pars1 = pars[1:ncol(U)]; pars2=pars[-(1:ncol(U))];
933     mu = U%*%pars1;
934     sigma = exp(pars2[1]+pars2[2]*mu);
935     dSN1(new.size, mu=mu, sigma=sigma, nu=pars2[3], log=TRUE)
936 }

```

937 Parameters and their standard errors can then be estimated with `maxLik`, starting
938 from a random guess:

```

939 start=c(runif(ncol(U)), rep(0,3))
940 out=maxLik(logLik=LogLik,start=start, new.size=simData$new.size,U=U,
941   method="BHHH",control=list(iterlim=5000,printLevel=1),finalHessian=TRUE);
942 coefs = out$estimate; # parameters
943 V = vcov(out); SEs = sqrt(diag(V)); # standard errors

```

944 In real life we would repeat the optimization several times with several different starting
945 values, to be confident that the optimal parameter values had been found.

946 Focus now on the year-specific intercept parameters $\hat{a}_t, t = 1, 2, \dots, T$. We can view
947 the year-specific estimates \hat{a}_t as consisting of unobserved true values a_t plus sampling
948 error:

$$949 \quad \hat{a}_t = a_t + \varepsilon_t \quad (\text{S.5})$$

950 Because of the sampling errors, the sample variance of the estimates \hat{a}_t is an upward-
951 biased estimate of the true across-year variance in the parameter. That is undesirable if
952 the model will be used to project how temporal variability affects population dynamics.
953 However, maximum likelihood estimation gives us an approximate variance-covariance
954 matrix \hat{V} of the sampling errors, V in the code above. With that information, we can
955 estimate the parameters of a random effects model for the intercept parameters, and
956 thereby improve the year-specific estimates and the estimate of the across-year variance.

957 The model is as follows. We make the standard mixed-models assumptions that the
958 a_t are drawn independently from some fixed distribution with unknown variance σ^2 .
959 We also assume that the estimates \hat{a}_t are unbiased, that is

$$960 \quad \mathbb{E}(\varepsilon_t | a_t) = 0. \quad (\text{S.6})$$

961 These are optimistic assumptions, but not excessively optimistic. Some degree of tem-
962 poral correlation will often be present, and as we explain at the end, it is theoretically
963 possible to account for it. Maximum likelihood parameter estimates are not unbiased,
964 but if the assumptions of maximum likelihood are satisfied the bias is asymptotically

965 negligible compared to the standard error (the bias scales as the inverse of sample size,
 966 the standard error as the square root of the inverse of sample size).

967 Let S^2 denote the sample variance of the estimates \hat{a}_t . It can then be shown that

$$968 \quad \mathbb{E}(S^2) = \sigma^2 + \frac{1}{T} \sum_{t=1}^T \mathbb{E}Var(\varepsilon_t) - \frac{1}{T(T-1)} \sum_{i=1}^{j-1} \sum_{j=1}^T \mathbb{E}Cov(\varepsilon_i, \varepsilon_j). \quad (\text{S.7})$$

969 This is eqn. (1) in Gould and Nichols (1998) in our notation, without the term that results
 970 from temporal autocorrelation.

971 The terms besides σ^2 on the right-hand are the expected impact of sampling error
 972 on the across-year variance of the parameter estimates; their presence makes S^2 a biased
 973 estimated of σ^2 . However, all of those terms correspond to entries in the variance-
 974 covariance matrix V . We can therefore use our estimated variance-covariance matrix \hat{V}
 975 to removes the bias due to sampling variability:

$$976 \quad \hat{\sigma}^2 = S^2 - \frac{1}{T} \sum_{t=1}^T \hat{V}_{t,t} + \frac{1}{T(T-1)} \sum_{i=1}^{j-1} \sum_{j=1}^T \hat{V}_{i,j}. \quad (\text{S.8})$$

977 $\hat{\sigma}^2$ estimates the variance of the distribution from which the a_t are assumed to be drawn.

978 Using that estimate, we can adjust the year-specific estimates to reduce the ex-
 979 pected impact of sampling error. Depending on your purposes, there are two possible
 980 adjustments. The first option is the one used in the popular capture-recapture analysis
 981 software Mark Cooch and White (2020),

$$982 \quad \tilde{a}_t = \bar{a}_t + \sqrt{\frac{\hat{\sigma}^2}{\hat{\sigma}^2 + \hat{V}_{t,t}}} (\hat{a}_t - \bar{a}_t). \quad (\text{S.9})$$

983 The name “shrinkage” comes from the fact that each estimate is adjusted towards the
 984 overall mean, with larger adjustments of values that have higher estimated sampling
 985 error variance, $\hat{V}_{t,t}$. This shrinkage estimate has the property that the expected sample
 986 variance of the adjusted estimates \tilde{a}_t is very close to $\hat{\sigma}^2$, so the \tilde{a}_t approximate the actual
 987 amount of parameter variation.

988 The second is to replace \hat{a}_t by the least-squares estimate of a_t under the additional
 989 assumption that the a_t are drawn from a Gaussian distribution; this is given by

$$990 \quad \tilde{a}_t = \bar{a}_t + \frac{\hat{\sigma}^2}{\hat{\sigma}^2 + \hat{V}_{t,t}} (\hat{a}_t - \bar{a}_t). \quad (\text{S.10})$$

991 This option is theoretically preferable if the Gaussian assumption is reasonable, and you
 992 are more interested in year-specific values rather than across-year variance. However,
 993 Metcalf et al. (2015) found that even (S.9), which does less shrinkage, resulted in a small
 994 downward bias in the temporal variance of population growth rates. This argues for
 995 always using the first option, and we do the same here.

996 We differ from MARK, however, in using (S.8) rather than an iterative method
 997 that takes (S.8) as its starting estimate and refines the estimate by using weighted least
 998 squares based on the current estimate. Metcalf et al. (2015) found, in simulation studies,
 999 that the iterative method was either slightly beneficial or wildly inaccurate. We therefore
 1000 advise against it.

1001 Finally, as mentioned above, the estimate of σ^2 can account for temporal autocor-
 1002 relation in the a_t . When present, those correlations add a term to eqn. (S.7) (see eqn.
 1003 (1) in Gould and Nichols (1998)), which can be estimated from the sample autocorre-
 1004 lation of the \hat{a}_t . We do not recommend doing this (and therefore omit the formulas)
 1005 because the autocorrelations can only be reliably estimated if they fall to nearly zero
 1006 within lag $m \ll T$, in which case the autocorrelation term is small (specifically, $O(m/T)$).
 1007 Otherwise, the random error from using poorly estimated autocorrelations is likely to
 1008 outweigh the small bias from omitting that term.

1009 The take-home message is that estimating random effects from the regression coef-
 1010 ficients is very simple:

```

1011 # Variance-covariance matrices for intercepts and slopes
1012 V1 = V[1:T,1:T]; V2 = V[(T+1):(2*T),(T+1):(2*T)];
1013 # Extract year-specific intercepts, center them to zero
1014 fixed.fx = coefs[1:T]; fixed.fx = fixed.fx-mean(fixed.fx);
1015
1016 # Estimate sigma^2
1017 var.hat = mean(fixed.fx^2) - mean(diag(V1)) +
1018           (sum(V1)-sum(diag(V1)))/(2*T*(T-1));
1019
1020 # Shrink deviations from the mean
1021 shrinkRanIntercept = fixed.fx*sqrt(var.hat/(var.hat + diag(V1)));
1022
1023 # Do it all again for the slopes
1024 fixed.fx2 = coefs[(T+1):(2*T)]; fixed.fx2 = fixed.fx2-mean(fixed.fx2);
1025 var2.hat = mean(fixed.fx2^2) - mean(diag(V2)) +
1026           (sum(V2)-sum(diag(V2)))/(2*T*(T-1));
  
```

```
1027 shrinkRanSlope = fixed.fx2*sqrt(var2.hat/(var2.hat + diag(V2)));
```

1028 The figure below shows the results for one artificial PSSP “data” set, having $T = 22$
1029 years and growth measurements on about 175 individuals/year on average. The true
1030 random year effects (the ones used to generate the data) are recovered with good accu-
1031 racy and no bias. In particular there is no sign of extreme values being pulled in too
1032 far towards the mean, which would cause an S-shaped graph of estimated versus true
1033 values.

